Politecnico di Torino

The Role of Agricultural Waste in Limiting the Leaching of Pesticides: Laboratory Insights

TESI DI LAUREA MAGISTRALE IN
ENVIRONMENTAL AND LAND ENGINEERING
INGEGNERIA PER L'AMBIENTE E IL TERRITORIO

Author: **MARYAM MOHAMMADTAHERI**

Advisor: Prof. Tiziana Anna Elisabetta Tosco
Co-advisor: Dr. Monica Granetto

July 2025

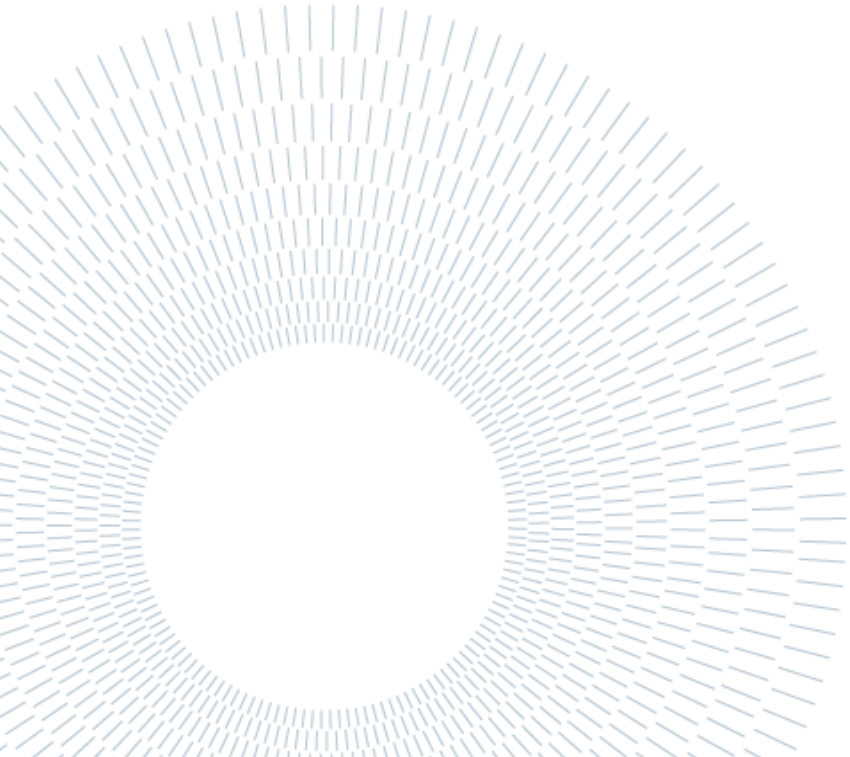

Abstract

The widespread uncontrolled use of agrochemicals has raised growing concerns about polluting groundwater and environmental matrices; however, they are essential for ensuring crop productivity. Consequently, there is a strong need for sustainable mitigation strategies.

This research explores agricultural waste-derived materials as sustainable adsorbents for pesticides in water and soil systems, focusing on their influence on contaminant leaching behavior. Wood-derived biochar, corncob-derived biochar, and raw corncob were chosen as sorbents for two representative agrochemicals: the herbicide Dicamba and the fungicide copper sulfate. A series of batch adsorption tests, kinetic adsorption, and column transport tests were conducted, supported by material characterization (pH, EC, bulk density), to assess the effect of different mixing ratios, solution volume, and the age of the material. Particularly, in batch tests, the adsorbents were in contact with the contamination in different concentrations. The results emphasize the higher adsorption capacity of biochar-based materials rather than others. Also, the results showed that a higher amount of amendments in the mixture leads to a higher adsorption.

Adsorption trends were obtained using UV-Vis spectrophotometry and HPLC as precise analytical techniques. Freundlich and Langmuir models were used for model fitting for Copper and Dicamba adsorption data, which showed strong alignment with Freundlich isotherms across all materials, with R^2 values exceeding 0.85 in most cases. This indicates multilayer adsorption and surface heterogeneity, which makes them sustainable agri-waste amendments for capturing agrochemicals.

Column leaching tests, which mimic contaminant transport in soil when amendments are applied, generated breakthrough curves that enabled the calculation of porous media characteristics and mass recovery. These results confirmed the effective retention of both contaminants, based on the pore volume time and baseline obtained from the tracer test. Following leaching, the column was sectioned at different depths to extract the retained copper and Dicamba and to determine their vertical concentration profiles.

These findings provide practical guidance for integrating low-cost, agri-based sorbents into environmental and land management strategies aimed at reducing agrochemical mobility in soil and water. This work contributes to the broader discussion on circular resource use and contamination mitigation in agricultural systems and groundwater.

Key-words: Agrochemical leaching, Biochar, Dicamba, Copper sulfate, Isotherm modeling, Column tests, Sustainable adsorbents, Agricultural waste

Abstract in Italiano

L'uso diffuso e incontrollato degli agrofarmaci ha sollevato crescenti preoccupazioni per l'inquinamento delle acque sotterranee e delle matrici ambientali; tuttavia, essi rimangono essenziali per garantire la produttività agricola. Di conseguenza, è fortemente necessario sviluppare strategie di mitigazione sostenibili.

Questa ricerca esplora l'utilizzo di materiali derivati da scarti agricoli come adsorbenti sostenibili per pesticidi nei sistemi suolo-acqua, concentrandosi sul loro effetto sul trasporto dei contaminanti nei suoli. Sono stati selezionati tre materiali adsorbenti: biochar derivato da legno, biochar derivato da tutoli di mais e tutoli di mais grezzi, applicati a due agrofarmaci rappresentativi: l'erbicida Dicamba e il fungicida solfato di rame. È stata condotta una serie di prove in batch per la determinazione delle isoterme e delle cinetiche di adsorbimento e test di trasporto in colonna, supportate dalla caratterizzazione dei materiali (pH, conducibilità elettrica, densità apparente), per valutare l'effetto di diversi rapporti di miscelazione e dell'età del materiale. In particolare, nei test in batch, i materiali adsorbenti sono stati messi a contatto con contaminanti a concentrazioni diverse. I risultati hanno evidenziato una capacità di adsorbimento maggiore nei materiali a base di biochar rispetto agli altri. Inoltre, è emerso che un maggiore contenuto di ammendanti nella miscela comporta un aumento dell'adsorbimento.

Le concentrazioni dei contaminanti studiati sono state analizzate mediante spettrofotometria UV-Vis e HPLC come tecniche analitiche di precisione. I modelli di Freundlich e Langmuir sono stati utilizzati per l'adattamento delle isoterme di adsorbimento di rame e Dicamba, mostrando una forte correlazione con l'isoterma di Freundlich per tutti i materiali, con valori di R^2 superiori a 0,85 nella maggior parte dei casi. Ciò indica un'adsorbimento multilayer e un'eterogeneità della superficie, il che suggerisce una buona performance dei materiali testati come ammendanti finalizzati alla rimozione dei contaminanti di origine agricola. Le curve di breakthrough ottenute dai test di trasporto in colonna, che simulano il trasporto dei contaminanti nel suolo in presenza di ammendanti, sono state analizzate per determinare, tra l'altro, le caratteristiche idrodinamiche del mezzo poroso, i meccanismi e parametri di trasporto e i bilanci di massa nelle diverse condizioni testate. I risultati hanno confermato una rimozione efficace di entrambi i contaminanti. Dopo il test di trasporto, la colonna è stata sezionata a diverse profondità per estrarre il rame e il Dicamba trattenuti, determinando i profili di concentrazione verticale.

Questi risultati forniscono indicazioni pratiche per integrare materiali adsorbenti per applicazioni in agricoltura a basso costo nelle strategie di gestione ambientale e del territorio, mirate a ridurre la mobilità degli agrofarmaci nel suolo e nelle acque. Questo lavoro contribuisce al dibattito più ampio sull'uso circolare delle risorse e sulla mitigazione della contaminazione nei sistemi agricoli e nelle acque sotterranee.

Parole chiave: Lisciviazione di agrofarmaci, Biochar, Dicamba, Solfato di rame, Modellazione isoterma, Test in colonna, Adsorbenti sostenibili, Rifiuti agricoli

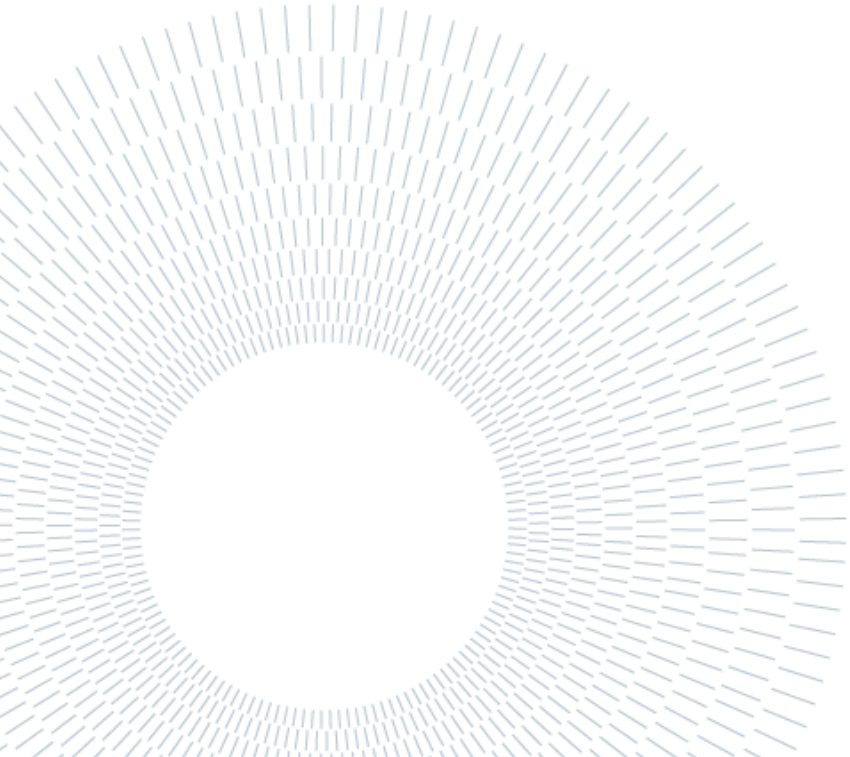

Contents

Acknowledgments

This publication is part of the NODES project, supported by the MUR PNRR MUR funds -M4C2 -Investment 1.5,'Ecosystems of Innovation' Notice, within the framework of the EU-funded PNRR -NextGenerationEU (Grant agreement No. ECS000036).

I would like to express my sincere gratitude to Professor Tiziana Tosco for her constant support, guidance, and insightful feedback throughout the course of this research. Her encouragement at every stage made this work possible.

A heartfelt thank you also goes to Dr. Monica Granetto, whose scientific expertise and previous research were instrumental in shaping both the experimental direction and the interpretation of the results. Her advice and availability were invaluable. Also, I must acknowledge the colleagues of the DISAT department, and particularly Dr. Francesca Demichelis, for providing the biochar.

I am deeply thankful to my family for their unwavering encouragement and emotional support throughout this journey, despite the physical distance between us.

Finally, I wish to thank my dear friends and everyone else who contributed in one way or another to this project. Your encouragement, feedback, and presence have been genuinely appreciated.

Introduction

The growing global population is placing high demand on agricultural systems to produce sufficient, healthy food. To meet this need, farmers widely rely on herbicides, fungicides and insecticides to enhance crop yields and ensure productivity. However, this intensive use of agrochemicals comes with environmental costs, as these substances often move beyond their intended targets. Through processes such as leaching, runoff, and volatilization, they can contaminate both soil and water bodies(((EEA), Soil pollution and ecosystems, 2018; Kookana, 2011; (USGS), 2022). The environmental fate of such chemicals depends on various factors, including soil type, chemical properties, and management practices (Sethi, 2019). At the same time, the increasing volume of agricultural production generates substantial amounts of organic waste, which presents its management challenges. In this context, an opportunity emerges to apply circular economy principles: transforming agricultural residues into functional materials that can help mitigate agrochemical pollution. This thesis explores the potential of using such waste-derived materials, specifically biochar and raw corncob, as natural sorbents to limit the environmental mobility of pesticides and heavy metals.

Dicamba, a benzoic acid herbicide commonly used in dicamba-tolerant crops, is known for its high solubility and mobility in soil. Although it degrades relatively quickly, its byproducts and persistence can still lead to groundwater contamination, especially in sandy or low-organic soils ((EPA), 2017; (MDA), 2019; Kah, 2014). On the other hand, copper sulfate, widely applied in vineyards and organic systems, is a heavy metal that can accumulate. Over time, it can accumulate in soils and eventually leach into water bodies once the soil's retention capacity is exceeded, particularly under acidic or light soil conditions.

To mitigate the environmental spread of agrochemicals, soil scientists are increasingly turning to natural amendments that improve the physical characteristics of soils. However, emerging research, including ours, explores the use of biochar as sorbents, not only in filtration systems but potentially also for in-soil applications aimed at reducing contaminant leaching. Two promising materials are **biochar**, a carbon-rich solid produced by pyrolysis of organic matter, and **raw corncob**, a lignocellulosic agricultural residue (Granetto M. B., 2024). Both are abundant, low-cost, and align with circular economic principles.

Biochar's porous structure, large surface area, and active surface functional groups make it an effective sorbent for both organic and inorganic pollutants (Ahmad, 2014; Spokas, 2012; Lehmann, 2015). Its performance, however, depends heavily on production conditions, including pyrolysis temperature and feedstock type, which influence its pore network and surface chemistry (Kan, 2016; Liu, 2017). Studies have shown that biochar can reduce leaching of compounds like 2,4-D, glyphosate, and copper under both lab and field conditions (Tong, 2019; Granetto M. B., 2024). However, only a few studies investigated their adsorption capacity toward agricultural contaminants such as pesticides (Cataldo, 2021).

Corncob, while less studied, also shows potential for agrochemical adsorption due to its high content of cellulose, hemicellulose, and lignin, which provide hydrogen bonding and hydrophobic interaction sites for herbicide molecules. It has long been used as a carrier for agrochemical formulations and can function as a low-energy, biodegradable sorbent (Granetto M. B., 2024). Recent comparative studies suggest that corncob may retain organic contaminants like dicamba more effectively than metals such as copper, which bind more strongly to biochar (Granetto M. B., 2024).

This thesis investigates the potential of **corncob and its derived biochar** to reduce the mobility of **dicamba** and **copper sulfate** in soil. The focus is on comparing the performance of the raw material with its thermally treated counterpart to understand the eventual advantages of the thermal treatment of the raw material. Also, our objective is to understand how these amendments influence pollutant transport under controlled conditions, using both equilibrium adsorption and dynamic flow testing. This approach aims to provide insights into low-impact strategies that combine environmental protection with sustainable agricultural practice.

1 General context and literature review

1.1. Introduction to Agri-Food Waste

1.1.1. Background and Definitions

Waste means any substance or object that the holder discards or intends or is required to discard (Magdalena Joka Yildiz, 2023). Among the various production processes, agriculture and the food industry are also responsible for waste production. Agro-food waste encompasses the organic residues generated throughout the agricultural and food processing sectors. This includes crop residues, fruit and vegetable peels, seeds, shells, and other by-products rich in organic matter and nutrients. The Food and Agriculture Organization (FAO) estimates that approximately one-third of all food produced globally is lost or wasted, amounting to about 1.3 billion tons annually ((FAO), Food Wastage Footprint: Impacts on Natural Resources, 2013). The global economic cost of food waste is estimated at $1 trillion annually, not accounting for environmental and social costs. This significant volume of waste presents both environmental challenges and opportunities for resource recovery.

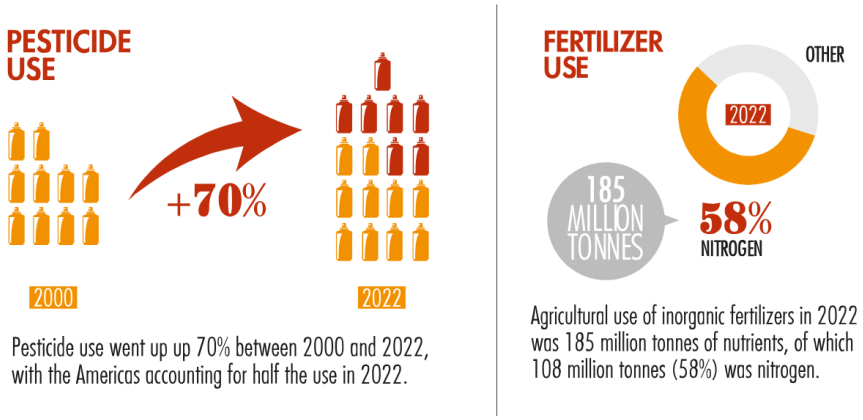

Figure 1 FAO chart for pesticide and fertilizer use (FAO statistics)

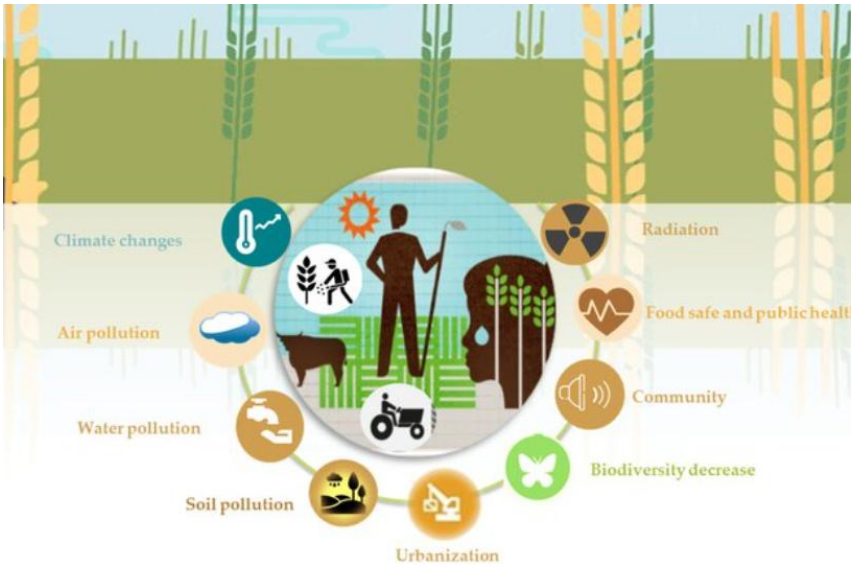

Figure 2 Agriculture's impact on the environment. (Cara, 2022)

1.1.2. Importance of Agri-Food Waste Management in Global Sustainability

The agri-food industry generates a significant amount of waste due to agricultural activities and industrial processing. These waste materials possess specific nutritional, fertilizing, and energy-related properties, which vary based on their origin and processing methods (Magdalena Joka Yildiz, 2023). Many plant-based wastes are rich in cellulose, hemicellulose, and lignin, making them suitable for biochar production and other valorization processes. On the other hand, the mismanagement of agro-food waste contributes to environmental degradation, including greenhouse gas emissions, surface and groundwater pollution, and soil degradation, including both diffuse emissions associated with excessive load of nutrients (in particular phosphorus and nitrogen), pesticides and pharmaceuticals (Dordio, 2013). Agricultural runoff containing fertilizers and organic waste contributes to nutrient pollution, leading to harmful algal blooms and dead zones in aquatic ecosystems. Traditional waste management, including methods such as anaerobic digestion, incineration, composting, utilization of fertilizer or animal feed, and landfilling, causes groundwater pollution through both leaching and infiltration, and air pollution through the emission of GHG, as well as dioxins and ash (Escudero-Curiel, 2023). The main research paths concerning the management of solid waste from the agri-food industry concerned their use as substrates for direct combustion processes (Magdalena Joka Yildiz, 2023). Additionally, these methods often fail

to recover valuable resources from waste, representing a lost opportunity for resource efficiency.

Effective management of agro-food waste is crucial for achieving global sustainability goals. By converting waste into valuable products like biochar, we can address multiple challenges simultaneously: reducing waste volumes, mitigating greenhouse gas emissions, and enhancing soil health. Additionally, controlling contaminant spread from diffuse sources is an intrinsically challenging target. To this aim, soil amendments, in particular processed or raw agricultural waste (e.g. sawdust, mowing, biochar, etc.) and minerals (e. g. zeolites) show good potential (Ahmad, 2014; Sud, 2008). Soil amendments, especially those made from processed or raw agricultural waste and minerals, have shown great potential in capturing and holding both organic and inorganic contaminants. These materials are already used in industries to treat polluted wastewater and to clean up contaminated soils and sediments (Cao, 2011; Ghosh, 2011). However, in farming, their main role so far has been to improve soil quality, helping the soil hold water and manage how fertilizers are released to plants (Diacono, 2010). This aligns with the principles of a circular economy, where waste is transformed into resources, promoting environmental sustainability and economic efficiency.

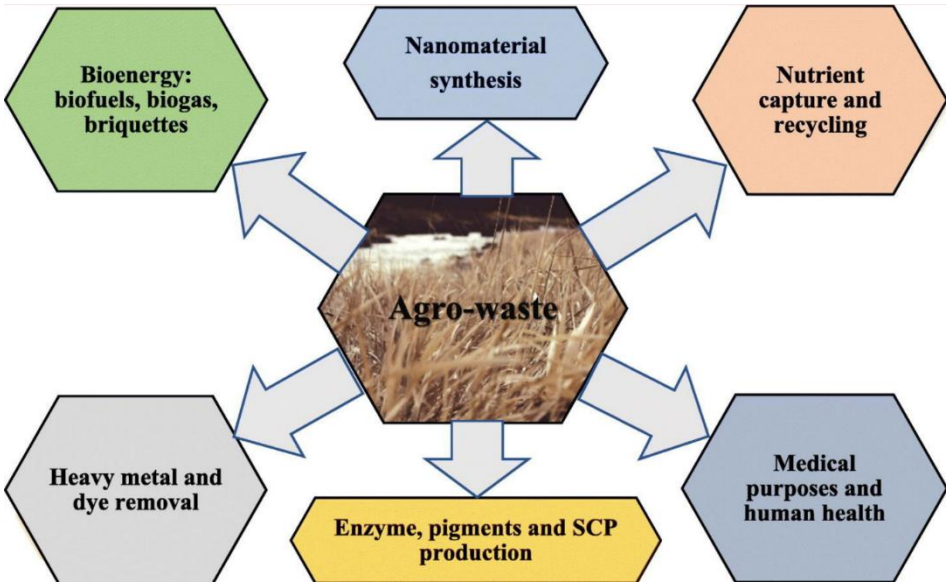

Figure 3 Valorization routes of agro-waste in sustainable applications, including bioenergy, nanomaterials, nutrient recovery, pollutant removal, and bioproduct development. (Dey, 2021)

1.2. Environmental impact of pesticide uses in agriculture

Pesticides, also called agrochemicals, include substances like insecticides, fungicides, herbicides, rodenticides, molluscicides, and nematicides. These chemicals play a crucial role in modern agriculture by reducing crop losses from the field to the consumer, and they also help to increase both the yield and quality of food in a cost-effective way (Tudi, 2021). Pesticides are essential in farming. Farmers depend on them to control weeds and insects in their crops, which has led to significant increases in agricultural productivity (Lamichhane, 2017). By use of pesticides, Since the early 20th century, agricultural yields have increased significantly to meet the demands of a growing population. According to the Food and Agriculture Organization (FAO), up to 40% of annual food crop production can be lost due to damage from pests and diseases ((FAO), International Year of Plant Health, 2020). Therefore, pesticides are essential in reducing these losses and helping to increase crop yields worldwide. Globally, pesticide production has grown by about 11% each year, rising from 0.2 million tons in the 1950s to more than 5 million tons by 2000 (Carvalho, 2017). Although pesticides have helped improve crop yields, their use has also been linked to several health concerns. These include acute and chronic issues such as respiratory (Ye, 2017), reproductive (Fucic, 2021), skin (Zendzian, 2003), gastrointestinal (Giambò, Teodoro, Costa, & Fenga, 2021), and neurobehavioral problems (Kori, 2018) associated with pesticide exposure. It has been estimated that when pesticides are applied in the field, about 60% to 70% of the chemicals do not reach their target, potentially spreading into the soil, water, and air (Gomes, et al., 2019).

Groundwater is an essential source of drinking water for much of the world's population. In Europe, around 65% of people rely on groundwater for drinking water ((EEA), 2022). However, this resource is under increasing threat from pesticide and nitrate leaching due to farming practices. Pesticides can reach groundwater through several pathways. One main route is infiltration from riverbeds and riverbanks, as pesticides applied to agricultural fields, urban areas, or other landscapes are carried by rainfall and irrigation water into nearby rivers and streams. Once in the water, pesticides can seep into the groundwater through the riverbed or banks. Another route is leaching, where pesticides applied to soil are carried down through the soil profile and unsaturated zone by water movement, eventually reaching the groundwater (Pérez-Lucas, 2018). These pathways pose serious risks because pesticides can persist in groundwater for long periods. The rate at which pesticides break down in groundwater is slower

than in surface water, increasing the risk of contamination to both human health and the environment.

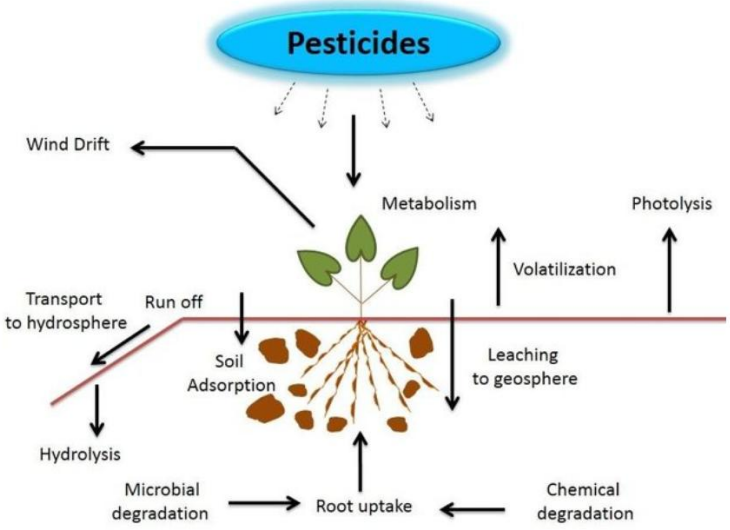

Figure 4 The environmental fate of pesticides (Ahemad, 2013)

1.2.1. Copper and dicamba

In this study, copper sulfate and dicamba were chosen as examples of inorganic and organic pesticides, respectively, both known for their high solubility and tendency to leach into the environment. Copper, as copper sulphate and other chelated or complexed forms is a fungiside used in agriculture and for direct application into aquatic systems with no toxicity concerns to humans when used according to label directions. Copper, widely used as a fungicide in organic farming, is recognized as a priority pollutant by the U.S. Environmental Protection Agency (USEPA). Its leaching behavior is influenced by factors such as the amount and duration of rainfall, the chemical properties of infiltrating water, like ionic strength and pH, and the presence of dissolved organic matter (DOM), which binds strongly with copper (Aldrich, 2002). In sandy soils, for example, up to 47.9% of copper has been reported to leach from columns containing 600 mg/kg of copper (Bakshi, 2014). Dicamba, a herbicide commonly used to control broadleaf weeds in crops like maize and sorghum, is highly soluble in water, which significantly increases its risk of leaching into soil and water systems (Granetto M. S., 2022). Other parts of the world, suggest an overall increase in the application of this herbicide in the next years (Aguiar, 2023).

This research aims to show how agri-food waste (milled corncob and CC biochar) might help reduce the leaching of soluble pesticides. Laboratory tests, including both batch tests and column transport experiments, were conducted to

understand how factors like the amendments' structure, composition, chemical properties, and how much applied affect pesticide adsorption and removal efficiency. While the study was carried out on the lab scale, it provided valuable early insights that could guide the use of these amendments in larger, real-world applications to immobilize pesticides in the soil.

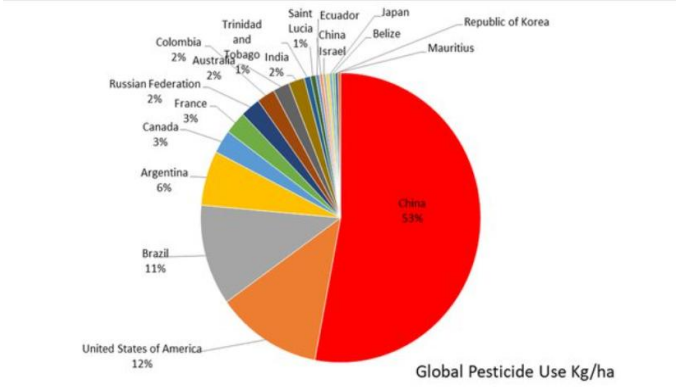

Figure 5 Global pesticide use (kg/ha) (data were taken from FAO-STAT 2022) (Cara, 2022)

1.3. Role of Biochar as a Sustainable Solution

Biochar production offers a promising pathway for the sustainable management of agro-food waste. Through pyrolysis, organic waste is converted into a stable form of carbon that can be applied to soils, improving fertility, water retention, and microbial activity. Additionally, biochar acts as a carbon sink, sequestering carbon in soils for extended periods and thus contributing to climate change mitigation.

Recent studies have highlighted the multifaceted benefits of biochar. For instance, biochar application has been shown to enhance soil water and nutrient retention capacity, increase crop yields, and improve microbial communities in various soil types (Pradhan, 2022). Furthermore, biochar produced from food waste has demonstrated effectiveness as an adsorbent for pollutants and as a means of reducing greenhouse gas emissions (Zhang, 2024; Agegnehu, 2016). Surprisingly, not much attention has been given to how these materials could interact with pesticides or help reduce the release of pollutants from agricultural sources (Kookana, 2011).

The production of biochar begins with the selection and collection of various biomass feedstocks, including agricultural residues, woody materials, sewage sludge, and organic waste. These raw materials undergo pre-treatment steps, such as drying, crushing, and sieving, to ensure uniformity and efficiency in the

conversion process. As illustrated in Figure 6, the pretreated biomass can then be transformed into biochar through several thermal conversion technologies, including pyrolysis (slow, intermediate, or fast), gasification, torrefaction, hydrothermal carbonization, or flash carbonization (Murtaza, 2021). Among these, pyrolysis is the most widely adopted method due to its simplicity and favorable yield of stable carbon-rich biochar

Biochar Production: Principles and Processes

Biochar is primarily produced through pyrolysis, a thermochemical process that decomposes organic biomass in an oxygen-limited environment, resulting in a carbon-rich solid along with bio-oil and syngas byproducts (Escudero-Curiel, 2023).The key parameters influencing the properties of biochar include pyrolysis temperature, heating rate, and residence time (Ge, 2024). Higher pyrolysis temperatures generally yield biochars with greater surface area and porosity but lower volatile matter content, enhancing their capacity for pollutant adsorption and carbon sequestration (Magdalena Joka Yildiz, 2023). By integrating biochar production into agro-industrial systems, waste streams can be valorized while simultaneously enhancing soil quality and reducing carbon emissions. This approach aligns with Sustainable Development Goals (SDGs), promoting resource efficiency and resilience in food systems (Magdalena Joka Yildiz, 2023).

Feedstock Selection and Preparation

The choice of biomass feedstock is crucial for biochar quality. Agro-food residues such as corncob, rice husks, fruit peels, and sawdust have been extensively studied due to their high lignocellulosic content, which enhances biochar stability and adsorption capacity (Ge, 2024; Nasiruddin Khan, 2007). Proper preprocessing, including drying and grinding, ensures consistent pyrolysis performance and product quality (Shen, 2004). The type of feedstock influences the chemical composition and structure of the resulting biochar. For example, woodworking-derived biochar exhibits a porous structure and high specific surface area, which contribute to its effectiveness in adsorbing heavy metals like copper and agrochemicals such as dicamba (Ge, 2024; Shen, 2004). The mineral content and inherent properties of the feedstock also affect the pH, cation exchange capacity, and nutrient availability in the biochar (Escudero-Curiel, 2023). Thus, selecting the appropriate feedstock is essential for tailoring biochar properties to specific environmental applications.

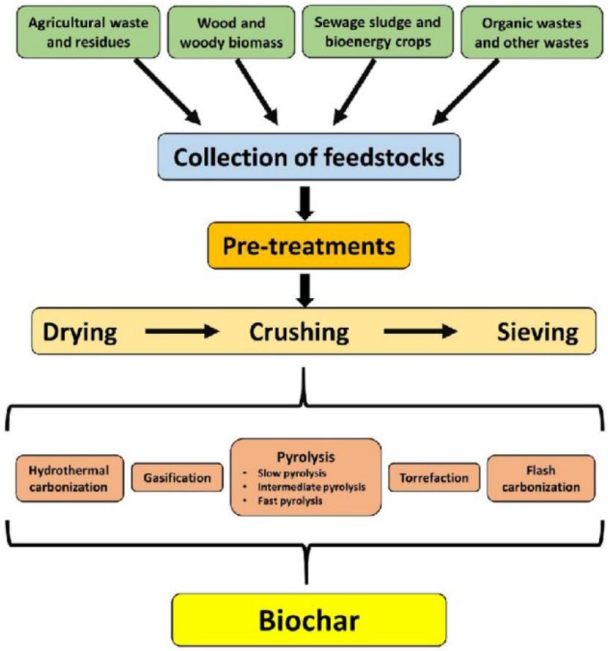

Figure 6 The flow chart diagram shows various steps (collection of feedstock, pre-treatments, and conversion into biochar through various processes) involved during biochar production from different organic wastes (Murtaza, 2021).

Biochar Characteristics and Functionality

Biochar's functionality is determined by its physical structure and chemical composition, key properties include porosity, surface area, pH, cation exchange capacity (CEC), and carbon stability (Escudero-Curiel, 2023). Biochar produced at higher pyrolysis temperatures tends to have a more porous structure and higher surface area, enhancing its ability to retain nutrients and adsorb pollutants (Magdalena Joka Yildiz, 2023). Additionally, biochar's alkaline nature and high CEC improve soil nutrient retention, supporting plant growth (Ge, 2024).

Stability and Carbon Sequestration Potential

One of biochar's most valuable properties is its long-term carbon stability. Pyrolyzed carbon structures are resistant to microbial degradation, enabling biochar to persist in soils for centuries (Ge, 2024). This stability not only supports soil amendment functions but also contributes significantly to carbon sequestration efforts, aligning with global climate change mitigation goals (Escudero-Curiel, 2023). By locking carbon into solid form, biochar mitigates atmospheric CO_2 accumulation, reducing the overall greenhouse gas burden (Joka Yildiz et al., 2023).

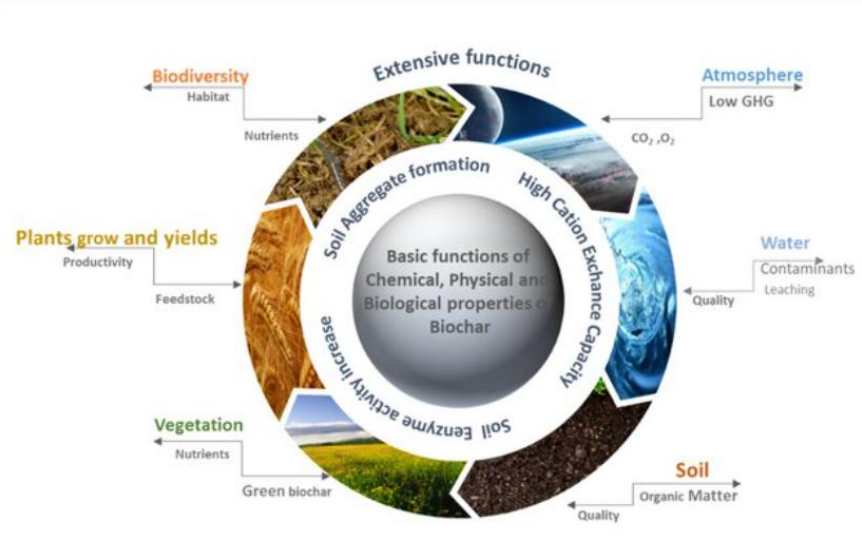

Figure 7 Environmental benefits of biochar (Cara, 2022)

Figure 7 illustrates the multifunctional role of biochar in agroecosystems, highlighting how its chemical, physical, and biological properties contribute to improved soil structure, enhanced nutrient cycling, pollutant retention, and broader benefits for water quality, plant growth, biodiversity, and climate mitigation.

Insights from Recent Literature

Emerging studies highlight advancements in biochar production and application. (Ge, 2024) reported that optimized pyrolysis conditions yield biochar with superior structural characteristics, improving its adsorptive performance. Moreover, recent work explores functionalizing biochar with nanomaterials and minerals to further enhance its environmental remediation capabilities (Escudero-Curiel, 2023). Novel reactor designs and decentralized biochar systems are also being developed to facilitate small-scale production and on-site application, addressing logistical challenges in rural and agricultural areas (Pradhan, 2022).

Identified Gaps in Current Research

While substantial progress has been made, critical gaps persist in understanding biochar's long-term interactions with soils, particularly under varying environmental conditions. Field-scale studies assessing biochar's effects on soil health, crop productivity, and carbon sequestration are limited and need expansion (Pradhan, 2022). Additionally, the potential risks associated with the accumulation of contaminants in biochar derived from heterogeneous waste streams warrant further investigation (Escudero-Curiel, 2023). More

interdisciplinary research combining agronomy, soil science, environmental engineering, and policy analysis is crucial to realize biochar's full potential.

1.4. Corncob as an agri-food waste

Corncobs are an abundant agri-food waste generated in enormous quantities alongside global corn production. Roughly 18% of the harvested corn grain mass ends up as corncob residue, amounting to well over a hundred million tonnes of waste annually. Traditionally, these lignocellulosic residues have found use as a bioenergy resource – they can be directly combusted or gasified to produce heat and power, offering a renewable fuel to offset fossil energy (Paulauskas, 2024). Corncobs have also been utilized in animal husbandry, for example, as a low-cost roughage or bedding material, though their nutritional value is limited. In industrial processes, corncobs serve as feedstock for biochemical production (notably for furfural and other furans), leveraging their high pentose content in biorefineries. These diverse applications exemplify efforts to valorize corn cob waste; however, a particularly promising avenue and the focus of recent research, is the conversion of corncobs into adsorbent materials for water and wastewater treatment.

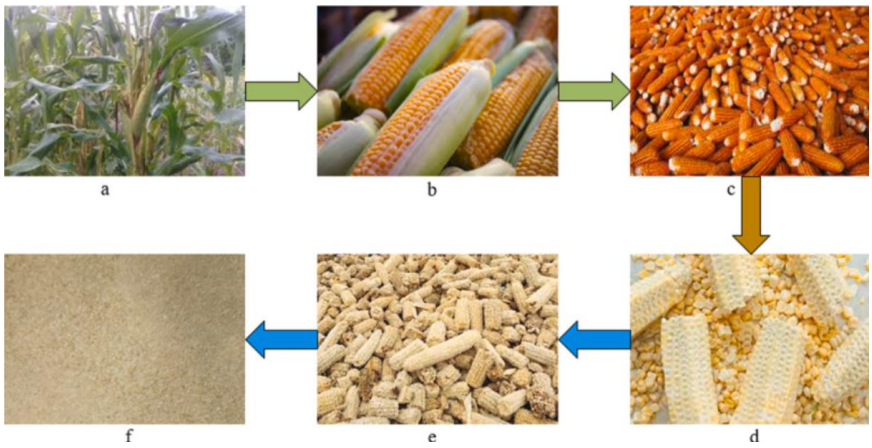

Figure 8 Material of corncob: (a) Corn plant, (b) Corn fruit, (c) Corn fruit before threshing, (d) Separation of corn kernels and cobs, (e) Corncob, (f) Corn cobs after milling (Gani, 2023)

Raw Corncob

Corncobs can be used in their raw or simply pretreated form (e.g. dried and ground into powder) as an adsorbent. Untreated corncob primarily contains cellulose, hemicellulose, and lignin with surface hydroxyl and carboxyl functional groups that can bind pollutants (Ahmed, 2023). Studies have shown raw or mildly modified corncob can uptake certain dyes and metal ions from

water, functioning as an eco-friendly biosorbent (Buasri, 2023). For example, raw maize cob powder has been tested for removing basic dyes like methylene blue and malachite green from solution, with measurable but relatively limited capacity (Buasri, 2023). Likewise, heavy metal adsorption using raw cob is feasible – e.g. nickel or lead ions can be scavenged to some extent by corn cob biomass – but the sorption capacities are generally low (often only on the order of a few mg of metal per gram of cob in batch tests) due to limited porosity and active site density (Chaudhari, 2022). To improve performance, simple chemical treatments can be applied: acid treatment (protonating and leaching soluble components) or alkali treatment (increasing surface negative charges) can enhance metal binding by exposing additional sorption sites. Overall, raw corncob biosorbents are low-cost and require little to no energy-intensive treatment, but their adsorption performance remains limited compared to that of thermally converted materials such as biochar and activated carbon (Ahmed, 2023). This has led researchers to convert corncobs into charcoals and activated carbons for higher efficiency.

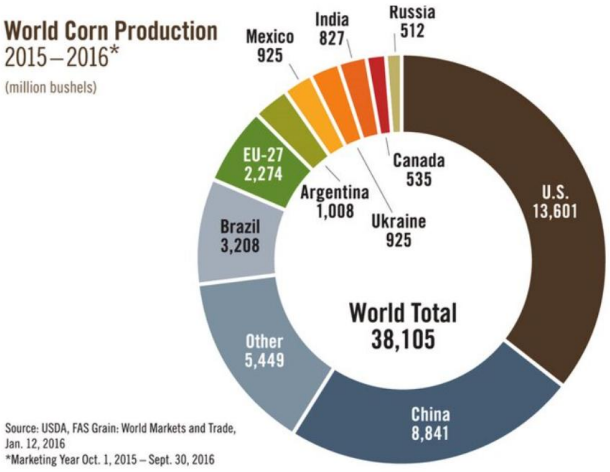

Figure 9 Global maize production (from World of Corn, 2016)

Corncob Biochar

Biochar produced from corncobs (often termed CC biochar) is obtained via pyrolysis of corncob under limited oxygen, typically at 300–700 °C. Corncob biochar exhibits substantially improved surface area and pore volume relative to raw corncob, which translates into greater adsorption capacity for pollutants (Gotore, et al., 2022). For instance, corncob-derived biochar has been reported as an effective adsorbent for heavy metals like chromium(VI) in water. In one recent study, optimized corncob biochar achieved a maximum Cr(VI) uptake of about 25 mg/g (Shakya, 2023). Corncob biochars have also shown good affinity for organic pollutants. They can effectively adsorb dyes and pharmaceutical compounds and hydrophobic partitioning within their carbon matrix (Gotore, et al., 2022). Although biochar works well as a soil amendment and an adsorbent, producing it requires a fair amount of energy. For a more sustainable approach, it would be better to use soil amendments made from agricultural waste that don't need a lot of energy to produce. One promising option is milled corncob, which is widely available and has a naturally porous structure. While corncob is mainly used for its energy content and as a raw material for biochar, there hasn't been much research on how effective raw, unprocessed corncob is as an adsorbent (Granetto M. B., 2024).

Copper adsorption on corncob

Table 1 summarizes the Langmuir and Freundlich isotherm parameters reported in the literature for copper adsorption onto various corncob-based adsorbents. The selected studies include both untreated corncob and chemically or physically modified forms (e.g., acid-activated, magnetically modified, biochar-derived). Across all cases, Langmuir models generally showed higher R^2 values, suggesting that monolayer adsorption mechanisms predominate on these materials. Adsorption capacities (q_{max}) varied widely depending on the adsorbent treatment, with values ranging from as low as 1–7 mg/g for raw corncob (Shen, 2004) up to 460.83 mg/g for PEI-modified magnetic corncob gel (Chen, 2022). Freundlich parameters further confirmed that surface heterogeneity plays a role, particularly in modified corncobs. This variability underlines the influence of surface modification, porosity, and functionalization on copper adsorption performance and highlights the potential for optimizing corncob-based materials for environmental applications.

Table 1 Freundlich and Langmuir parameters in different papers for copper adsorption of corncob

Reference	Corncob treatment	Langmuir			Freundlich		
		q_m (mg/g)	$K_{L\ (l/g)}$	R^2	$K_f((mg/g)*(l/mg)^{1/n})$	n	R^2
(Granetto M. B., 2024)	Raw corncob (untreated)	16	~0	High and better	~0	1.11	-
Shen & Duvnjak (2004)	Raw corncob (untreated)	1–7	0.02–0.11	-	-	-	-
(Nasirudd in Khan, 2007)	H_2SO_4-treated corncob (chemically activated)	31.45	-	0.98	-	-	-
(Lestari, 2020)	Magnetically modified corncob (Fe_3O_4-coated)	60.48	0.005	0.95	0.70	1.16	0.99
(Chen, 2022)	PEI-modified magnetic corncob gel (PEI-CC@Fe_3O_4)	460.83	2.94×10^{-3}	0.9965	8.036	1.77	0.98
(Saadi, 2024)	H_3PO_4-activated corncob carbon (AC-CC)	53.56	-	~0.94	-	-	0.95

2 Materials and Methods

2.1. Materials

The adsorbent materials used in this study were biochar, corncob, and medium silica sand, while copper sulfate and Dicamba served as the target agrochemical contaminants.

Four amendment materials were used in this study: two batches of corncob and two types of biochar. The corncobs were obtained from Agrindustria (Cuneo, Italy) at two different points in time. The biochars included one commercial product from Ronda Engineering (Italy) and one synthesized in the laboratory at DISAT – Politecnico di Torino, using the new corncob batch as feedstock. All materials were used in both pure form and mixed with quartz sand for adsorption and column tests. Their detailed characteristics are summarized in Table 2.

Table 2 Description of Amendment Materials Used in This Study

Material	Type	Time of Acquisition	Preparation/Properties
Old Corncob	Raw agricultural waste	December 2022	Fibrous part of corn ear; sieved to 180–610 μm and 610–850 μm
New Corncob	Raw agricultural waste	February 2024	Same origin; sieved to 180–610 μm and 610–850 μm
Commercial Biochar	Wood-drived biochar	-	From untreated woodworking waste; nominal size < 5 mm
Lab-Synthesized Biochar	Corncob-derived biochar	March 2024	Pyrolyzed at 400–600 °C, 10 °C/min heating rate, 30 min residence, under N_2 (0.4 mL/min); dried at 60–70 °C; sieved < 2 mm

Washed silica sand (Dorsilit 8 and Dorsilit 5G, supplied by Dorfner GmbH, Germany) by Ultrasonic Cleaner (CP102) was used to mimic the soil structure, as pure material or mixed with the amendments. The cleaning procedure is detailed in (Beryani, 2022). Dorsilit 8, with a d50 particle size of 0.45 mm, was used in mixture preparation, while Dorsilit 5G was used in column packing to ensure a stable base and top layer.

The selected contaminants used in both adsorption and column transport tests were copper(II) sulfate pentahydrate ($CuSO_4 \cdot 5H_2O$) and Dicamba (3,6-dichloro-2-methoxybenzoic acid, CAS No. 1918-00-9). Copper(II) sulfate pentahydrate was used as a model inorganic contaminant and was purchased from Scharlab (Spain) with a purity >99.5%. Dicamba, used as a model organic herbicide, was obtained from Alfa Chemistry (Ronkonkoma, NY, USA) with a minimum purity of 98%.

For copper quantification, Zincon Monosodium Salt (Alfa Aesar) ($C_{20}H_{15}N_4NaO_6S$) was used as a colorimetric method in UV-Vis spectrophotometric analysis. Potassium Bromide (KBr) (Chem-Lab) was used as a non-reactive tracer in column tests to determine hydraulic parameters such as pore volume and residence time. In all the steps of study, ultrapure deionized water was produced using a Milli-Q Pure Water System (Merck Millipore).

2.2. Methods

2.2.1. Characterization of the amendments

The three amendments were then individually mixed with sand at application rates of 5% and 20% by mass. The mixtures were hand-mixed thoroughly until fully homogeneous. To characterize them, bulk density, pH, and electrical conductivity (EC) were measured for the pure amendments, pure sand, and the sand-amendment mixtures. These measurements followed the protocols outlined in the European Biochar Certificate (EBC) guidelines for sustainable biochar production (Schmidt, 2015).

Bulk density was obtained by measuring the volume of a known amount of dry material in a graduated cylinder after compression. The bulk density is calculated as the ratio of the mass to the volume of the sample. The theoretical porosity can be calculated with the bulk density of the mixtures and mass according to the following equation:

$$\varphi = \frac{V - \frac{M_s}{\rho_s} - \frac{M_b}{\rho_{pa}}}{V} \qquad \text{eq1}$$

With M_s the mass of sand [M], M_b the mass of amendment [M], ps the sand particles' density [ML^{-3}], and ρ_{pa} the amendment particles' density [ML^{-3}].

The pH of the sample was measured by adding 5 grams of air-dried material by Precision Balances Precision Balances (Ohaus Pioneer, Ohaus Corporation, USA; Biltek Analytical Balance, Biltek Instruments, Italy) to 25 milliliters of a 0.01 M calcium chloride solution ($CaCl_2$, Alfa Aesar, purity ≥99%), giving a solid to liquid ratio of 1:5 (w/v). This mixture was placed in a volumetric flask and shaken gently for an hour using an overhead rotator to ensure proper mixing(Savatec Model, FALC Instruments, Italy). After the shaking, the pH of the suspension was measured using a pH meter (XS pH 70 Vio, XS Instruments, Italy).

The salt content of the sample was estimated by measuring its electrical conductivity. For this, 5 grams of air-dried sample were mixed with 50 milliliters of deionized water (a solid-to-liquid ratio of 1:10 w/v) in a volumetric flask. The mixture was gently rotated for one hour, following the same procedure as for the pH measurement. After shaking, the sample was centrifuged at 7000 RPM for 10 minutes using a bench-top centrifuge (Neya 16, G.V.I. S.p.A., Italy). It was then filtered using a 0.45 µm PTFE syringe filter (Thermo Fisher Scientific, Waltham, USA) to remove any particulates. The electrical conductivity of the filtered solution was then measured using an EC meter (MULTI340i with Tetracon 325 probe, WTW GmbH, Germany).

(a)

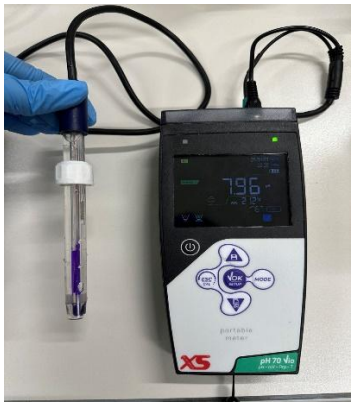

(b)

Figure 10 (a) EC meter (MULTI340i with Tetracon 325 probe) (b) PH meter (XS pH 70 Vio, XS Instruments)

2.2.2. Analytical method for Copper and dicamba Quantification

Copper concentration was measured using a colorimetric method based on a modified version of the approach by (Ghasemi, 2003), as adapted by (Granetto M. B., 2024). In this method, Zincon was used as a copper-binding agent, maintaining a molar ratio of 2:1 (Zincon:Cu), which resulted in a blue-colored solution. Calibration was achieved by preparing solutions with varying concentrations of Cu(II) while keeping the Zincon concentration constant, and the color change was measured at a wavelength of 605 nm using a UV-Vis spectrophotometer, Specord 600 (Analytik Jena, Germany), after a waiting time of 15 minutes. For each sample, 1 mL of the 1 mM Zincon solution is added to achieve the required copper concentration. To calculate the copper sulfate dilutions using the formula:

$$C_0 V_0 = C_f V_f \qquad \text{eq2}$$

Where C_0 and C_f are the initial and final concentrations of the solution, and V_0 and V_f are the initial and final volumes of the solution.

We assumed copper sulfate concentrations for calibration as follows: 0.05, 0.04, 0.03, 0.02, 0.01, 0.008, 0.006, 0.004, 0.003, and 0.002 mM. For each dilution, deionized water was added until reaching a final volume of 10 ml. The absorption spectra of the Cu-Zincon complex at different copper concentrations and the corresponding calibration curve at 605 nm are reported in Figures 18 and 19 in the results section.

High-Performance Liquid Chromatography (HPLC) (Shimadzu Nexera X2 HPLC System, Japan) was used to measure the concentration of Dicamba in the samples. To ensure accurate quantification, calibration curves were generated for this purpose. The dilution factor for each sample was calculated by weighing the amount of solution used to reach the desired final concentration. The calibration curve was prepared using standard solutions of Dicamba at concentrations between 10 ppm and 500 ppm. The calibration curve at 208 nm is shown in Figure 20 in the results section.

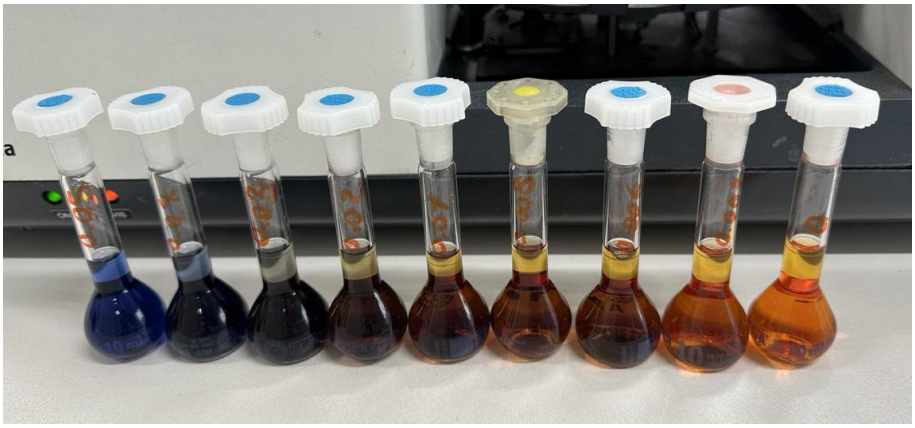

Figure 11 copper detection with Zincon

2.2.3. Batch adsorption test

Batch adsorption experiments were conducted to evaluate the capacity of selected adsorbent materials, pure biochar, pure corncob, and their mixtures with sand, to remove copper (Cu^{2+}) and Dicamba under controlled laboratory conditions. All batch tests were performed in 2 mL plastic vials. For each test, 100 mg of adsorbent was weighed and placed into the vial. For copper adsorption tests, solutions were prepared by diluting a 30 mM copper sulfate stock solution to cover a wide range of concentrations, from 0.1 mM to 30 mM. For Dicamba adsorption tests, the starting solution was a 2000 ppm (2 g/L) stock solution, from which a series of dilutions was prepared. The vials were placed on an overhead rotating shaker (FALC Overhead Rotator, Savatec Instruments Scientific, Italy) to ensure homogeneous mixing and continuous contact between the solid adsorbent and the liquid phase. The samples were agitated for 24 hours to allow the adsorption process to reach equilibrium. At the end of the contact period, the vials were centrifuged at 7000 RPM for 10 minutes (Neya 16 Bench Top Centrifuge, G.V.I. S.p.A., Italy) to separate the solid and liquid phases. The supernatant was then carefully filtered through 0.45 µm PTFE syringe filters to remove residual suspended particles. Copper concentrations were analyzed by UV-Vis spectrophotometry at λ = 605 nm, using the method described in the previous part. Dicamba concentrations were measured using High-Performance Liquid Chromatography (HPLC) as explained before. The amount of copper and Dicamba adsorbed was calculated according to the following relation:

$$s_{eq} = \frac{c_0 v_0 - c_{eq} v_{eq}}{w} \qquad \text{eq3}$$

With s_{eq} amount of contaminant adsorbed per unit weight of adsorbent [MM^{-1}], C_0 and C_{eq} initial and equilibrium contaminant's concentration in liquid phase [ML^{-3}], V_0 and V_{eq} initial and at equilibrium solutions' volume and W adsorbent weight [M].

After calculating the adsorbed amount of contaminant per gram of adsorbent from the initial and final solution concentrations, the equilibrium adsorption data were analyzed by fitting to two widely used models: Langmuir isotherm model, which assumes monolayer adsorption on a homogeneous surface and Freundlich isotherm model, which assumes adsorption on heterogeneous surfaces with varying affinities.

Langmuir equation:

$$S_{eq} = \frac{q_{max} L C_{eq}}{1 + L C_{eq}} \quad \text{eq4}$$

where $qmax$ is the maximum adsorption capacity [M/M] and L the Langmuir adsorption coefficient [l/mg].

Freundlich Equation:

$$S_{eq} = K_f \, C_{eq}^{\,1/n} \quad \text{eq5}$$

Where S_{eq} is the adsorbed concentration at equilibrium with the liquid concentration C_{eq}, K_f is the adsorption capacity ((mg/g) ×(l/mg)$^{1/n}$), and 1/n is the Freundlich constant. The adsorption behavior is classified as follows:

- 1/n<0.1 → Strongly favorable adsorption
- 0.1<1/n<0.5 → Favorable adsorption
- 1/n>0.5 → Unfavorable adsorption

The best-fitting model is determined by comparing R^2 values, indicating whether monolayer (Langmuir) or multilayer (Freundlich) adsorption is dominant.

In addition to the main batch adsorption tests, two sets of additional experiments were performed to further investigate specific factors that could influence the results. First, I conducted a volume effect assessment, since in the study by (Granetto M. B., 2024), batch tests were performed using 50 mL vials with 2.5 g of adsorbent, whereas my standard procedure was carried out in 2 mL vials with 100 mg of adsorbent. To check whether the vial volume (and consequently the solid-to-liquid contact conditions) could affect the adsorption behavior, I repeated selected batch tests using both volumes under the same conditions.

Secondly, some other batch tests were performed on different materials. For instance, I performed batch tests on newly purchased pure corncobs. This was done to verify whether the age of the material had any effect on adsorption performance, as the laboratory also had a stock of pure corncob that had been stored for about two years. Comparing the adsorption behavior of the new and aged corncob allowed me to evaluate the potential impact of material ageing on the adsorption of copper and Dicamba.

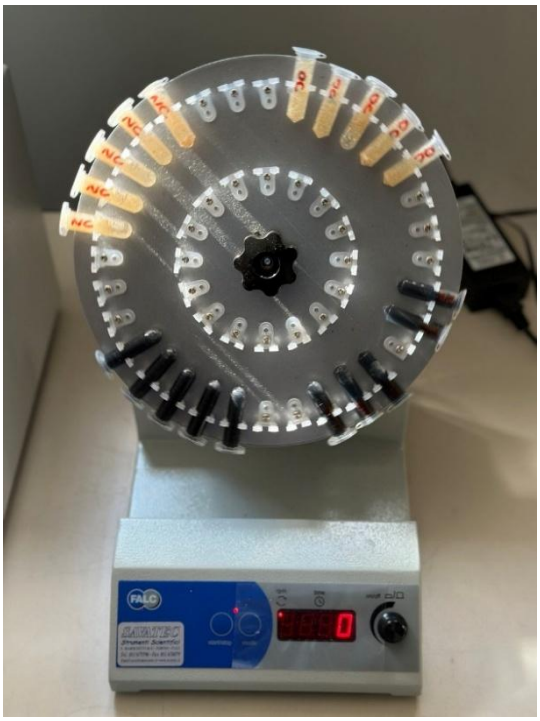

Figure 12 The overhead shaker used during the batch adsorption tests for sample mixing

In the next step, kinetic adsorption tests have been performed to determine the time at which adsorption reaches equilibrium conditions. The same procedure as the batch equilibrium tests was followed, but instead of a single contact time (24 h), the adsorption process was monitored at different time intervals (e.g., 15 min, 30 min, 1 h, 3 h, 6 h, 24 h). The time-dependent adsorption data were then fitted to several kinetic models: Pseudo-first-order model, Pseudo-second-order model, and Elovich model. The pseudo-first-order kinetic model, first proposed by Lagergren in 1898 (Revellame, 2020), assumes that the adsorption rate of a contaminant is directly proportional to the difference between the amount adsorbed at equilibrium and the amount adsorbed at any given time (Revellame, 2020). This model follows the equation:

$$\frac{dq}{dt} = k_1(q_e - q) \quad \text{eq6}$$

where q is the mass of adsorbate on the sorbent at time *t*, q_e is the equilibrium adsorbed amount, and k1 is the first-order kinetic constant. The model is linked to a linear driving force (LDF), where the rate of adsorption decreases as equilibrium is approached. A low value of k_1 or a small difference (q_e-q) results in a slower adsorption process. The model can be linearized as:

$$ln(q_e - q) = \ln q_e - k_1 t \quad \text{eq7}$$

Allowing the parameters k_1 and q_e to be estimated from experimental data. The pseudo-second-order kinetic model, first introduced by Ho in 1996 (Ho, 1999), assumes that the rate of adsorption depends not only on the amount of contaminant already adsorbed but also on the number of available adsorption sites on the sorbent surface. The model is expressed by the following equation:

$$\frac{dq}{dt} = k_2(q_e - q)^2 \quad \text{eq8}$$

where q is the adsorbed amount at time t, q_e is the equilibrium adsorbed amount, and k_2 is the pseudo-second-order kinetic constant. Upon integration and linearization, the model can be expressed as:

$$\frac{t}{q} = \frac{1}{k_2 q_e^2} + \frac{t}{q_e} \quad \text{eq9}$$

The Elovich model (Kajjumba, 2018), introduced in 1939, is often used to describe chemisorption processes on heterogeneous surfaces. It is particularly suitable when the adsorption surface contains sites with varying energy levels. The model has been widely applied in studies involving the adsorption of metal ions such as Cu^{2+}, Co^{2+}, Ni^{2+}, and Zn^{2+} onto materials like resins and activated carbon (Wu, 2009). The Elovich model is expressed by the equation:

$$\frac{dq}{dt} = ae^{-bq} \quad \text{eq10}$$

where a is the initial adsorption rate and b is the desorption constant. After integration and linearization, the model takes the form:

$$q = \frac{1}{b}\ln(abt) = \frac{1}{b}\ln(ab) + \frac{1}{b}\ln(t) \quad \text{eq11}$$

By plotting the amount adsorbed q as a function of ln(t), the constants a and b can be estimated.

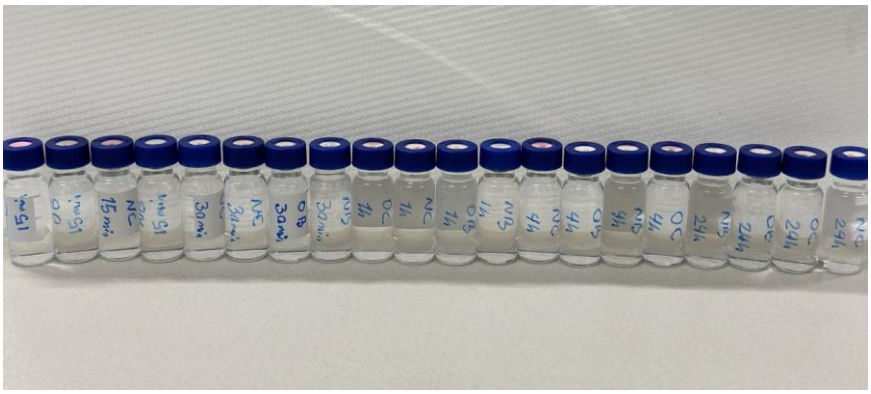

Figure 13 Dicamba kinetic adsorption

2.2.4. Column transport test

2.2.4.1. Column setup and packing

For the column tests, Dorsilit 8 silica sand (d_{50} = 0.45 mm) was used as the base packing material. To improve flow stability and minimize disturbance at the inlet and outlet, a ~2 cm layer of Dorsilit 5G (d_{50} ≈ 0.7mm) sand was placed at both ends of the column. The tests were carried out using glass columns with an internal diameter of 4.1 cm. For each test, 320 g of dry sand or sand–amendment mixture (containing 5% amendments by weight) was prepared. In particular, due to the limitation of the pyrolysis of corncob biochar, we had to reduce the length of the column to 15cm. Thus, 240g of the mixture of cc biochar and sand (12g cc biochar in each column) was used. To improve the cohesion and facilitate packing, the amendment mixture was pre-wetted by adding 5% of the total dry weight of deionized water. Before packing, the pump flow rate was set at 0.36 mL/min, which corresponded to 9 RPM on the peristaltic pump. This value was used to calculate the Darcy velocity by having the cross section of the column (0.00045 cm/s). The column was packed using a slow upward flow to maintain full water saturation during the process. The material was introduced layer by layer and gently compacted to avoid air gaps or bubbles inside the column.

2.2.4.2. Tracer test

For the tracer tests, a 10 mM potassium bromide (KBr) solution was prepared and used as a conservative tracer. To enable conversion from EC to concentration, a calibration line was first established by measuring the EC of a series of KBr solutions at known concentrations. The initial concentration (C_0) for each test was determined by measuring the EC of two 10 mL vials of the tracer solution using a calibrated EC meter. For the saturated tracer test, a downward flow was applied at the set flow rate (0.36 mL/min) for a minimum of 8 hours. The breakthrough curve (BTC) was generated by collecting effluent samples at fixed intervals and measuring their EC, then plotting the normalized concentration (C/C_0) against time (min). Once the curve reached a stable plateau, indicating complete tracer breakthrough, deionized water (DW) was injected to flush the column. After flushing, the tubes were detached, and the column was left to drain by gravity, allowing the system to transition to unsaturated conditions.

To initiate the unsaturated tracer test, DW was first injected to confirm flow control and system stabilization under the same conditions. The KBr solution was then reinjected at the same flow rate, and the outlet EC was recorded to produce a second BTC in unsaturated condition. A final DW flush completed the unsaturated tracer sequence.

The pore volume time was estimated from each BTC by first determining the average EC values at the baseline and the plateau. The midpoint between these two values was identified, and the corresponding time at which the BTC reached this midpoint was taken as the pore volume time. This value was then corrected by subtracting the tubing time, which had been measured earlier, to obtain the actual pore volume time for the system.

2.2.4.3. Column leaching test

The column leaching tests were carried out by injecting copper sulfate pentahydrate (2.5 mM) and Dicamba (2 g/L) solutions into separate columns packed with either pure sand or a sand mixture containing 5% corncob by weight. Each solution was injected continuously for 24 hours under controlled flow conditions, except in columns with the mixture of sand and cc biochar, injection of dicamba and copper sulfate lasted for 40 hours to reach the plateau of the breakthrough curve. The outflow from the columns was collected using a fraction collector, including overnight sampling, to ensure continuity of data. The collected samples were later analyzed. UV-Vis spectrophotometry was used for copper analysis, while High-Performance Liquid Chromatography (HPLC) was used for Dicamba analysis. For both analyses, a calibration curve was generated

from freshly prepared standard solutions to obtain the relation between wavelength and the concentration of the solution, ensuring accuracy in concentration calculations and enabling precise mass balance analysis of the breakthrough curves (BTCs). Some samples of the injected solution were also analyzed as C_0 to normalize the BTC data by plotting C/C_0 versus time. In addition, the pore volume time was calculated from the tracer test and used to determine the approximate time when the contaminant front began to saturate the column, providing insight into the transport behavior and retention characteristics of the adsorbent media.

Figure 14 column transport test setup

3 Results and Discussion

3.1. Characterization of the adsorbent material

The properties of the amendments, commercial biochar, CC biochar and corncob (both in old and new batches), were first characterized in terms of bulk density, electrical conductivity (EC), and pH, as these parameters are known to influence both adsorption behavior and the potential application of amendments for agrochemical.

The results of the bulk density measurements are shown in Figure 15. Corncob exhibited the highest bulk density values, with an average of 533.91 ± 40.34 g/L for the new corncob and 539.44 ± 14.17 g/L for the old corncob. The similarity between old and new batches indicates that this property is relatively stable despite minor differences in particle size and ageing. Commercial biochar showed lower bulk density values, typical of highly porous carbonaceous materials. The commercial biochar presented an average of 337.22 ± 2.55 g/L, while the corncob-driven biochar exhibited a slightly higher value of 350.56 ± 8.22 g/L. This slight increase is consistent with the higher degree of compaction observed visually in the new batch and in line with values reported in the literature.

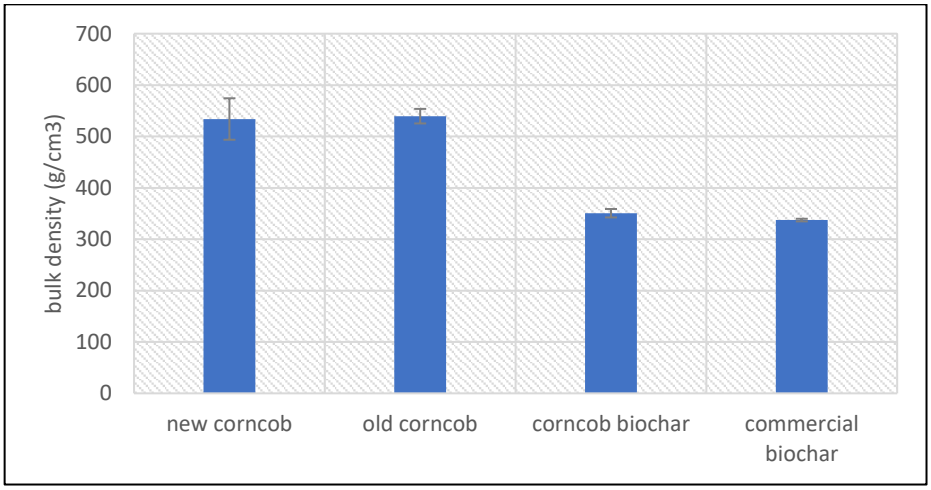

Figure 15 bulk density of the adsorbent materials

The EC of the amendments is reported in Figure 16. The new corncob showed an average EC of 593.33 ± 29.48 µS/cm, average is slightly higher than the old corncob (540.00 ± 56.57 µS/cm).The variances (error bars) of the two ranges overlap, so there is no statistically significant difference between the values for the two samples. Biochar presented a very clear difference between commercial and corncob-drived batches. The old commercial biochar had an EC of 211.33 ± 7.09 µS/cm, while the corncob biochar showed a markedly higher value of 649.00 ± 15.56 µS/cm. This strong increase is consistent with higher ash content and the possible presence of more soluble salts in the corncob-dreived biochar, an effect that has been frequently observed when commercial biochar is obtained from heterogeneous commercial residues (Spokas, 2012).

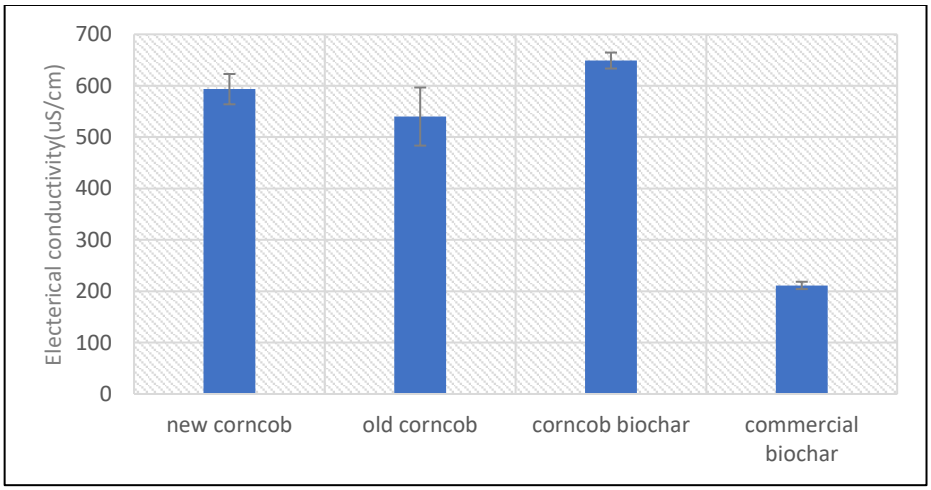

Figure 16 EC of the adsorbent materials

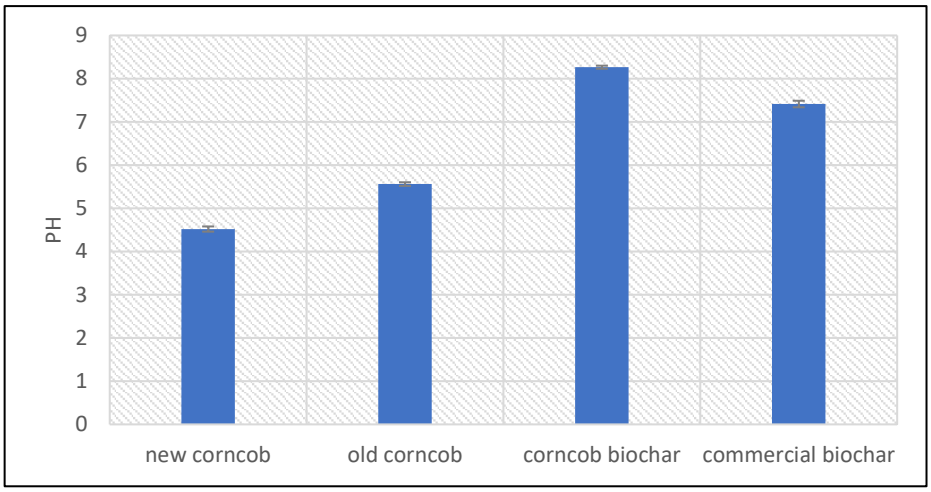

Figure 17 PH of the adsorbent materials

The pH values are shown in Figure 17. Corncob exhibited acidic behavior, with pH values of 4.52 ± 0.06 (new batch) and 5.56 ± 0.04 (old batch). The lower pH of the new corncob suggests a higher presence of organic acids or other acidic groups, possibly due to differences in the procedure of drying and milding. Biochar exhibited alkaline behavior, in agreement with previous findings. The commercial biochar showed an average pH of 7.41 ± 0.08, while the cc biochar had an even higher value of 8.27 ± 0.04, consistent with higher ash content and greater basicity. This trend is known to enhance the electrostatic interaction with cationic species such as Cu^{2+} but may also slightly reduce the affinity for acidic organic compounds such as Dicamba under certain pH conditions.

Overall, these results confirm that commercial biochar and corncob can provide complementary properties when used as soil amendments. Biochar, with its high pH and high EC, is likely to be more effective for cation adsorption (Cu^{2+}), while corncob, with its lower pH and higher organic content, is expected to provide better interaction with acidic herbicides such as Dicamba, an observation consistent with previous works.

3.2. Copper and dicamba determination

Figure 18 shows the UV-Vis spectra of Zincon-Cu(II) complexes recorded in the 180–800 nm wavelength range, confirming the presence of a clear absorbance peak at 605 nm, with the highest part belonging to 0.05 mM copper. The corresponding calibration curve is reported in Figure 19. A linear correlation (R^2 = 0.9949) was obtained in the tested concentration range, ensuring reliable quantification of Cu(II) in the adsorption tests. This calibration line is used in the adsorption batch tests and copper detection in the column tests.

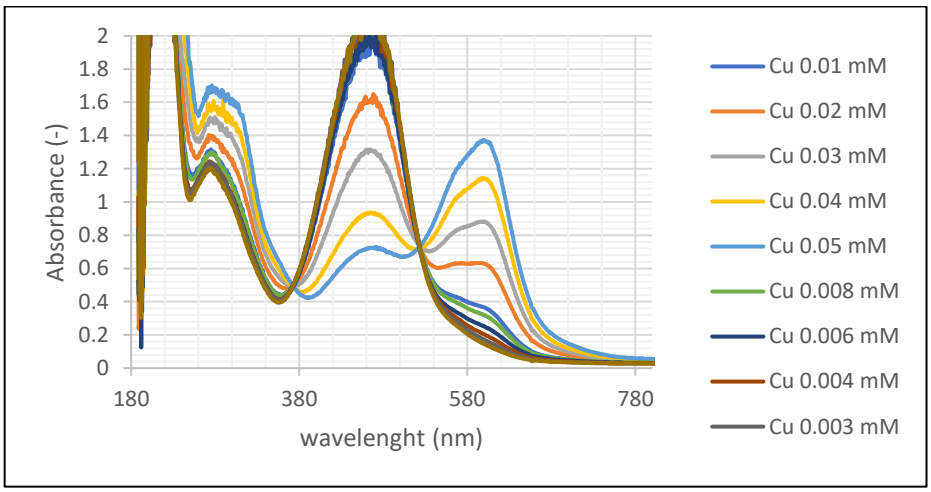

Figure 18 Zincon-Cu complexes measured with UV-Vis spectrophotometer (Specord S600, Analytik Jena, Germany) for Cu(II) concentration from 0.003 mM to 0.01 mM in the wavelength range 250-800 nm

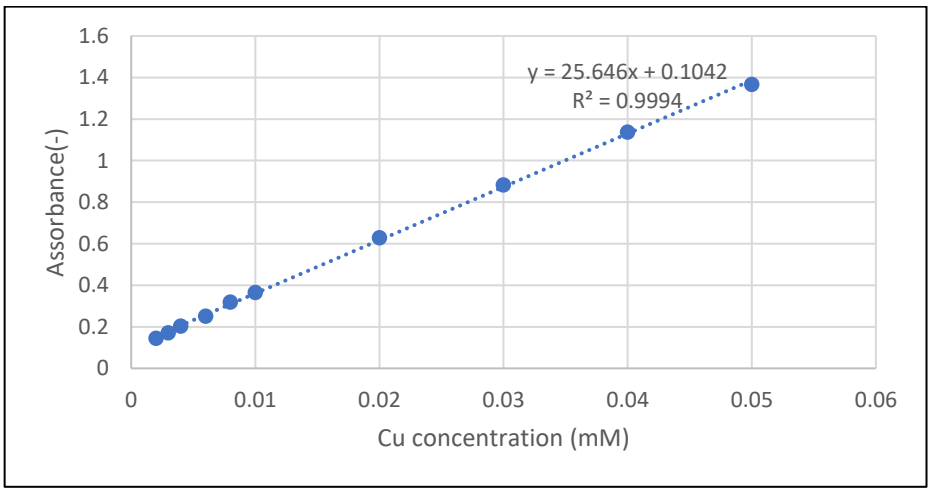

Figure 19 Calibration curve of Zincon-Cu complexes measured with UV-Vis spectrophotometry at λ = 605 nm

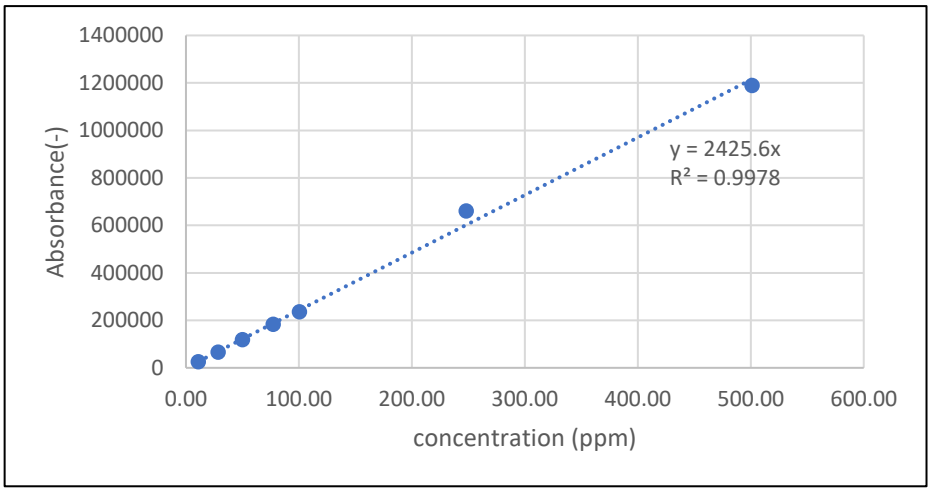

Figure 20 Calibration curve of Dicamba solutions measured with HPLC at λ = 208 nm

Figure 20 reports the calibration curve obtained for Dicamba. A good linear correlation was observed (R^2 = 0.9978), demonstrating the reliability of the method for concentration determination in the adsorption experiments.

Both analytical methods showed excellent linearity within the working ranges selected for the batch adsorption tests.

3.3. Batch adsorption test

3.3.1. Kinetic adsorption (Copper sulfate)

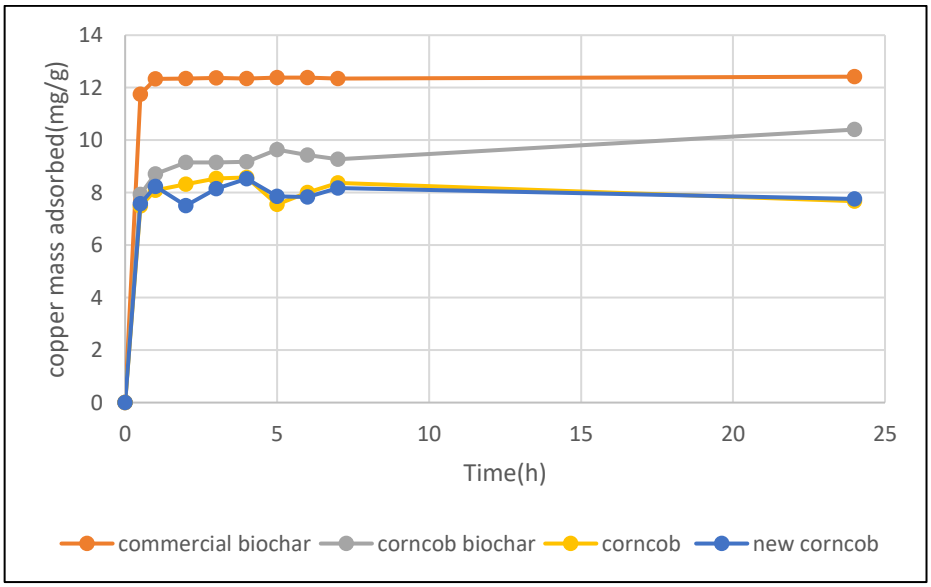

Figure 21 Kinetic adsorption of copper sulfate on pure adsorbent materials

First, kinetic adsorption tests were performed to determine the time required to reach equilibrium conditions at a constant concentration of 2.5 mM copper sulfate. The results are shown in Figure 21, which reports the copper mass adsorbed (mg/g) over time for all tested amendments.

The adsorption capacity followed the trend: commercial biochar > corncob biochar > corncob ≈ new corncob. This behavior is consistent with the results obtained later in the equilibrium adsorption tests. commercial biochar exhibited the highest adsorption capacity, with values close to 13 mg/g, and equilibrium was reached very rapidly, within 15 minutes. This result agrees with previous studies reporting fast adsorption kinetics for biochar, with more than 95% of Cu^{2+} adsorbed within the first hour (Mahdi, 2018). For corncob biochar, the adsorption kinetics were slower, but the material still reached adsorption capacities above 10 mg/g after approximately 24 hours. The slower kinetics compared to commercial biochar can be attributed to the lower surface area and possibly less accessible adsorption sites, as also observed in other studies (Ge, 2024). Corncob and new corncob both displayed similar kinetic behavior, with initial adsorption being relatively fast (within the first few hours), but a slight decrease in adsorption capacity was observed over time, stabilizing around 8 mg/g. This behavior may be explained by partial desorption or rearrangement of Cu^{2+} on weaker adsorption sites, a phenomenon previously reported for lignocellulosic materials.

Table 3 Kinetic model fitting parameters for copper adsorption on biochar, corncob biochar, corncob, and new corncob.

	Pseudo-first order model		
	k_1 (h^{-1})	q_e (mg/g)	R^2
New corncob	-	-	-
Corncob	-	-	-
Corncob biochar	-	-	-
Commercial biochar	-	-	-
	Pseudo-second order model		
	k_2 (mg/g h)	q_e (mg/g)	R^2
New corncob	1.13	7.75	0.99
Corncob	0.62	7.63	0.99
Corncob biochar	0.08	12.07	0.99
Commercial biochar	3.87	12.42	1
	Elovich model		
	a (mg/g)	b (mg/g h)	R^2
New corncob	$1.31.10^{-49}$	13.54	0.04
Corncob	$2.18.10^{-22}$	5.73	0.18
Corncob biochar	10080.90	1.13	0.74
Commercial biochar	$3.06.10^{+22}$	41.47	0.62

As shown in Table 3, the pseudo-first order model did not adequately describe the experimental data for any of the tested materials, as no meaningful fitting parameters or valid R^2 values were obtained.

Conversely, the pseudo-second order model provided an excellent fit for all materials, with R^2 values higher than 0.99 for all samples, reaching 1.000 for biochar. The highest equilibrium adsorption capacities (q_e) were obtained for biochar (12.43 mg/g) and corncob biochar (12.07 mg/g), confirming the trend already observed in the kinetic curves (Figure 22). Corncob and new corncob exhibited similar q_e values of approximately 7.64–7.75 mg/g.

The Elovich model provided acceptable fits only for biochar-based materials, with moderate R^2 values (0.748 for corncob biochar and 0.624 for commercial biochar), suggesting the presence of heterogeneous surface sites and chemisorption processes, in agreement with the high surface complexity of these materials. For corncob samples, the Elovich model showed poor fitting ($R^2 < 0.2$), indicating that physical adsorption or weaker interactions likely dominate in this case. A contact time of 24 hours was ultimately selected for the batch tests to ensure that the adsorption capacity of the materials was fully reached.

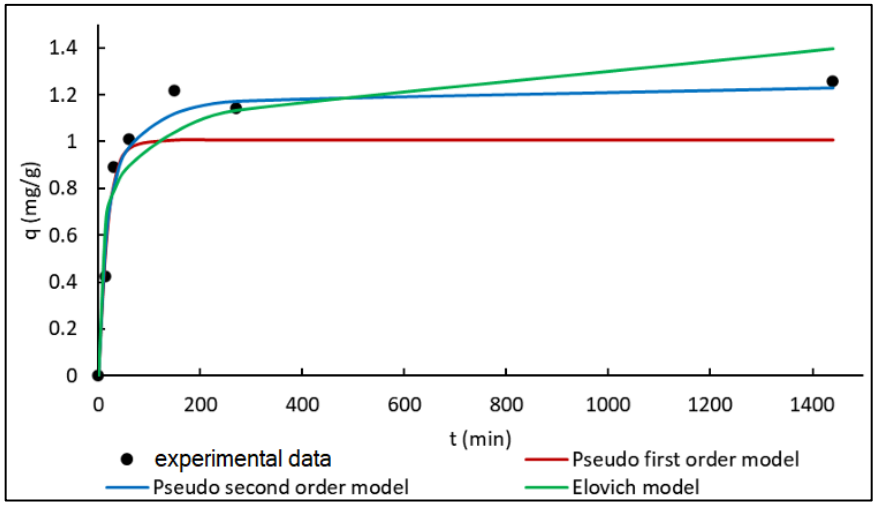

Figure 22 An example of experimental data fitting (in black) with pseudo-first order (in red), pseudo-second order (in blue), and Elovich model (in green)

3.3.2. Equilibrium adsorption (Copper sulfate)

3.3.2.1. Effect of different mixing rates of amendments

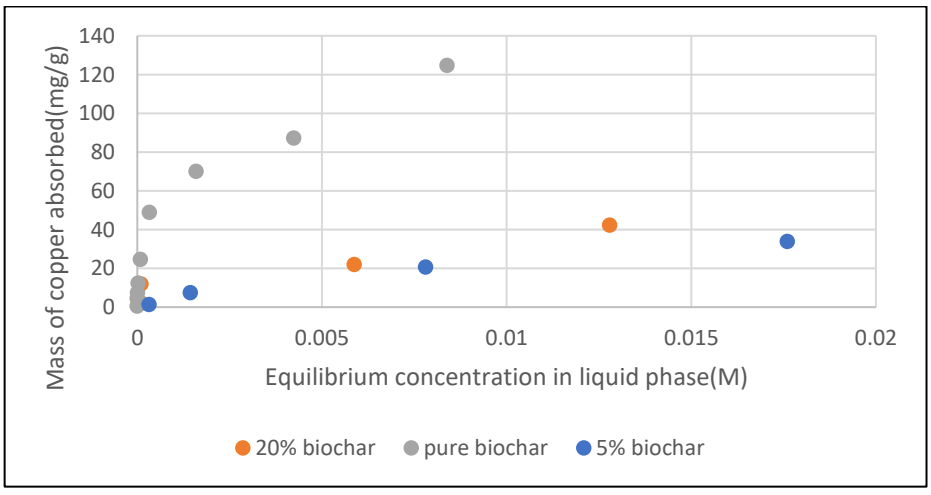

Figure 23 Equilibrium adsorption of copper sulfate on pure and mixed biochar at 5% and 20% amendment rates.

Equilibrium adsorption tests were performed to evaluate the effect of amendment content on the adsorption capacity of copper sulfate. Mixtures of 5% and 20% amendment (biochar or corncob) with sand were compared to the corresponding pure amendments. The results are shown in Figures 23 and 24.

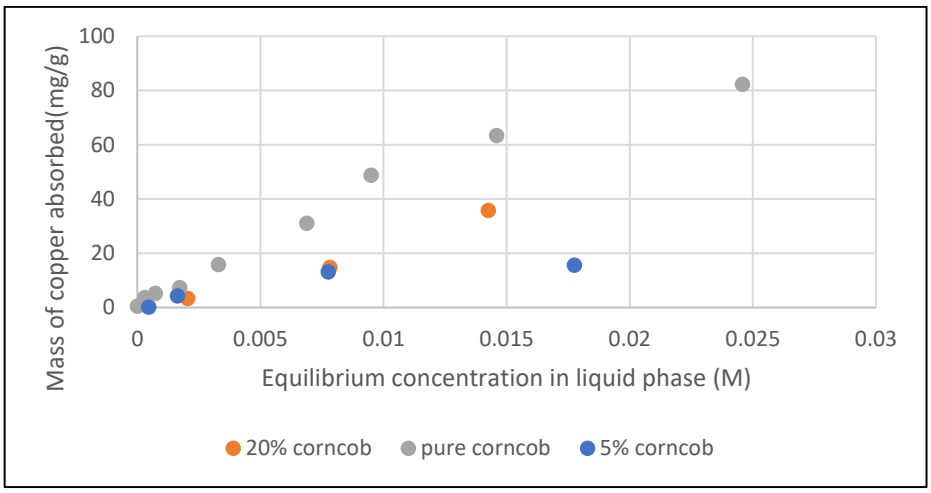

Figure 24 Equilibrium adsorption of copper sulfate on pure and mixed corncob at 5% and 20% amendment rates.

For both materials, a clear decrease in adsorption capacity was observed with decreasing amendment content. As expected, pure biochar and pure corncob exhibited the highest adsorption capacities, while mixtures with 20% and especially 5% amendment showed progressively lower adsorption performance. For biochar (Figure 23), pure biochar reached adsorption capacities exceeding 130 mg/g, while 20% and 5% biochar mixtures exhibited maximum capacities of approximately 40–50 mg/g and 20–30 mg/g, respectively. A similar behavior was observed for corncob (Figure 24), with maximum adsorption capacities of approximately 80 mg/g for pure corncob, compared to 20–30 mg/g for the 20% mixture and even lower values for the 5% mixture.

3.3.2.2. Aging effect on corncob

The effect of aging on the adsorption capacity of corncob was evaluated by comparing the performance of old pure corncob and new pure corncob. The results are shown in Figure 25. A negligible difference in adsorption behavior was observed between the two materials. The old corncob exhibited a slightly higher adsorption capacity, reaching values of approximately 80 mg/g at the highest equilibrium concentration tested. In contrast, the new corncob showed lower adsorption capacities, with a maximum of approximately 50 mg/g.

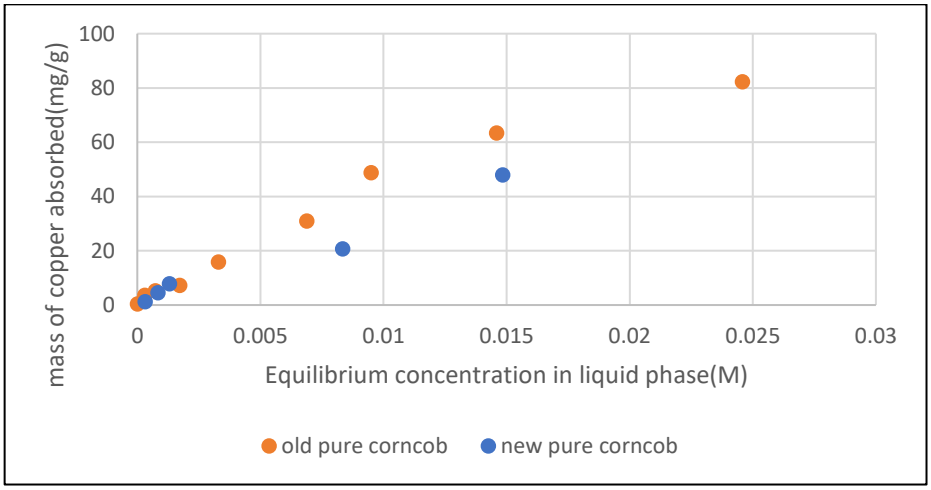

Figure 25 Equilibrium adsorption of copper sulfate on old and new pure corncob.

3.3.2.3. Volume effect

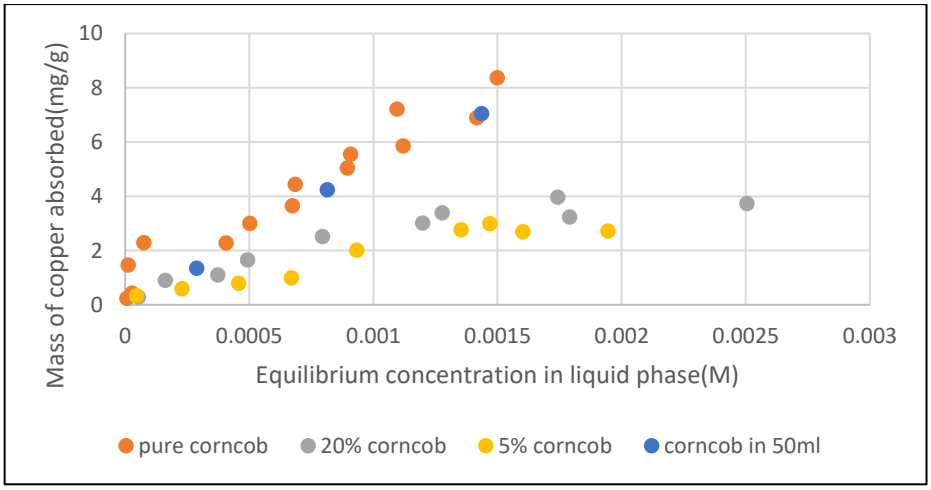

Figure 26 Effect of volume on copper adsorption onto pure corncob

The experiments aimed to assess whether varying both the solution volume and the solid/liquid ratio would influence the adsorption process. The results for Corncob and biochar are shown in Figures 26 and 27, respectively.

For corncob (Figure 26), the adsorption capacities obtained in 50 mL for pure corncob were slightly lower than those measured in the 2 mL tests. The difference became more evident at higher equilibrium concentrations. This suggests that under the tested conditions, the adsorption process on corncob may be influenced by the combined effect of solution volume and adsorbent mass, likely due to differences in mass transfer and availability of adsorption sites per unit volume.

For biochar (Figure 27), a similar trend was observed: adsorption capacities in the 50 mL for pure biochar tests were slightly lower than those in 2 mL, particularly at low equilibrium concentrations. This may be explained by the slower diffusion of Cu^{2+} ions in the larger solution volume, combined with the higher mass of adsorbent, which can result in more complex adsorption dynamics.

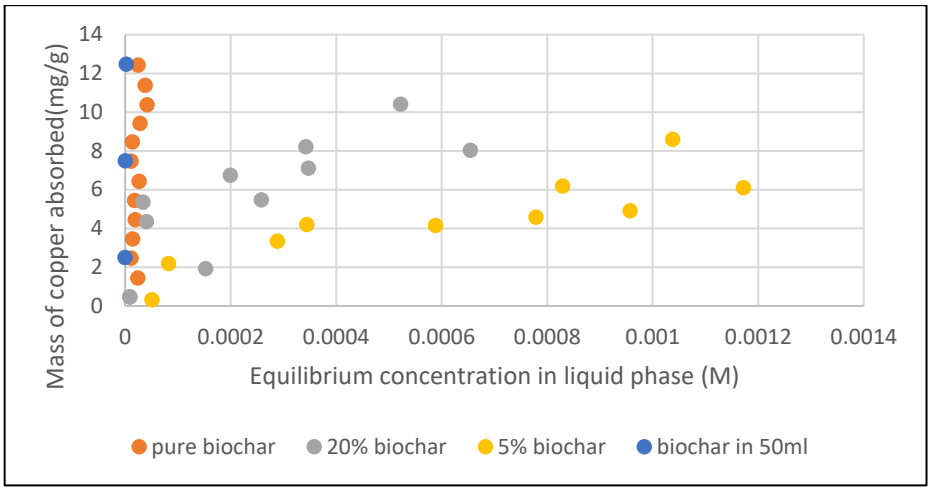

Figure 27 Effect of volume on copper adsorption onto pure biochar

Overall, these results indicate that the volume effect and the associated change in solid/liquid ratio can have a low impact on copper adsorption performance, particularly for biochar and at low equilibrium concentrations. Thus, the 2ml volume for these tests can effectively evaluate the adsorption performance of the adsorbent materials.

3.3.2.4. Comparison of all materials

Finally, a comparison was performed between all tested materials to assess their overall copper adsorption performance under equilibrium conditions. The tests were conducted in 24h of contact time in 2ml vials to evaluate the adsorption performance of the materials. Among the tested amendments, commercial biochar exhibited the highest adsorption capacity, with values exceeding 130 mg/g at the highest equilibrium concentration tested. This confirms the excellent performance of biochar for copper removal, as also observed in previous studies. New biochar also showed good performance, although slightly lower than the biochar, with maximum adsorption capacities around 80–100 mg/g. The difference between the two batches may be explained by variations in surface chemistry, pore structure, and ash content, as discussed in Section 3.1. Old

corncob exhibited intermediate behavior, reaching maximum adsorption capacities of approximately 80 mg/g, very similar to the new corncob.

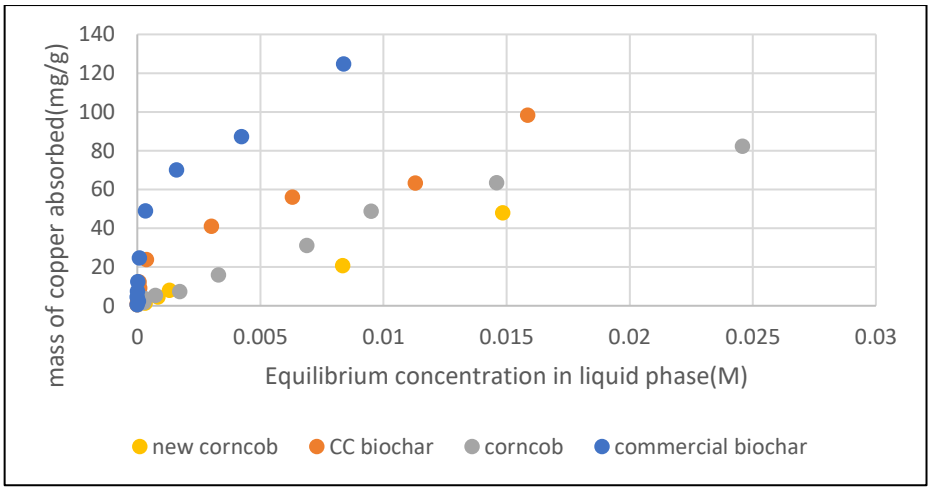

Figure 28 Comparison of copper adsorption performance of new corncob, CC biochar, corncob, and commercial biochar.

Overall, the materials followed the adsorption capacity trend:

Commercial biochar > CC biochar > Old corncob > New corncob

Shown in figure 28, Commercial biochar exhibited the highest copper uptake in both kinetic and equilibrium conditions, indicating a strong and rapid adsorption capacity. Corncob biochar showed intermediate performance, with a slower but still increasing trend in the kinetic test and moderate capacity in the isotherm data. These results highlight the superior affinity of biochar-based materials for Cu (II) adsorption, likely due to their high surface area and the presence of functional groups promoting strong metal binding. In contrast, corncob-based materials, while still providing measurable adsorption, exhibit lower capacities, consistent with their lower surface area and more heterogeneous surface chemistry.

To better describe the adsorption equilibrium behavior of Cu (II) on the tested amendments, the experimental data were fitted using both the Freundlich and Langmuir isotherm models. The fitting parameters are reported in Table 4. The Freundlich model provided good fits for most materials, with R^2 values generally higher than 0.9, except for pure biochar ($R^2 = 0.78$), where the Langmuir model showed poor correlation, possibly due to the presence of heterogeneous adsorption sites and multilayer adsorption phenomena (shown in Figure 29).

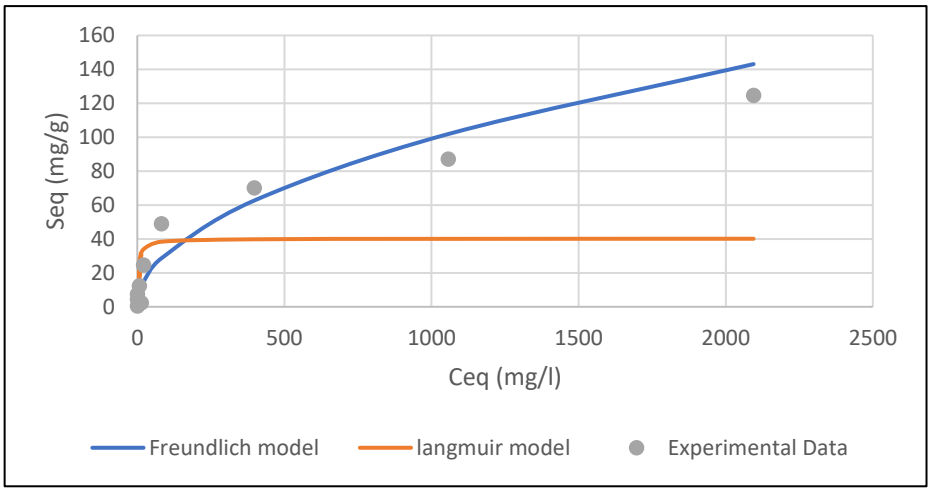

Figure 29 experimental data fitting with the Freundlich (in Blue) and Langmuir (in Orange) models for commercial pure biochar

For biochar-based materials, adsorption followed the Freundlich model better than Langmuir, confirming the complex surface chemistry and heterogeneity of these materials. The 1/n values for biochar (around 0.5) indicate a favorable adsorption process, consistent with strong metal binding reported for biochar. In contrast, corncob-based materials showed a better fit with the Langmuir model (R^2 = 0.87–0.98), indicating a tendency toward monolayer adsorption on more homogeneous surfaces. The calculated q_{max} values for pure and new corncob (around 53–56 mg/g) confirm the good capacity of corncob for Cu^{2+} adsorption, although lower than that of pure biochar (40 mg/g) and especially commercial biochar (130 mg/g, Section 3.3.2.4). As expected, the mixtures (5%, 20%) exhibited lower q_{max} values due to the dilution effect already discussed in Section 3.3.2.1.

Table 4 Freundlich and Langmuir parameters obtained from copper sulphate isotherm modelling

	Freundlich			Langmuir		
	1/n (-)	K_f $((mg/g)*(l/mg)^{1/n})$	R^2 (-)	q max (mg/g)	L(l/g)	R^2
Corncob biochar	0.55	1.10	0.95	8.52	$1.56.10^{-01}$	0.92
New corncob	0.84	$4.30.10^{-02}$	0.96	56.83	$2.96.10^{-04}$	0.98
Pure corncob	0.72	$1.41.10^{-01}$	0.97	53.46	$6.17.10^{-04}$	0.87
20% corncob	0.80	$3.40.10^{-02}$	0.95	6.04	$3.70.10^{-03}$	0.96
5% corncob	0.73	$3.50.10^{-02}$	0.95	2.45	$1.24.10^{-02}$	0.96
Commercial biochar	0.50	3.20	0.78	40.21	$2.54.10^{-01}$	0.92
20% biochar	0.49	$7.66.10^{-01}$	0.89	19.07	$1.21.10^{-02}$	0.78
5% biochar	0.66	$1.56.10^{-01}$	0.95	20.41	$1.49.10^{-03}$	0.89

After screening of four conditions on copper adsorption: volume effect, material aging, and comparison of mixed and pure materials, for Dicamba adsorption, due to the limited availability of adsorbents, the tests were focused only on the volume effect and comparison among the four selected materials in the equilibrium adsorption part.

3.3.3. Kinetic adsorption (Dicamba)

Kinetic adsorption tests were performed to evaluate the dynamics of Dicamba on the four selected amendments in 2ml vials: commercial biochar, CC biochar, corncob, and new corncob. Given the high precision of HPLC measurements, the kinetic tests were conducted in four replicates, and the results reported in Figure 30 represent the average values with standard deviations. All materials showed a very fast initial adsorption phase, with the majority of Dicamba being adsorbed within the first few hours. Corncob biochar and corncob exhibited slightly higher initial adsorption capacities, reaching values around 15–20 mg/g. In contrast, biochar and new corncob showed slightly lower adsorption capacities in the same time range, with values around 12–15 mg/g.

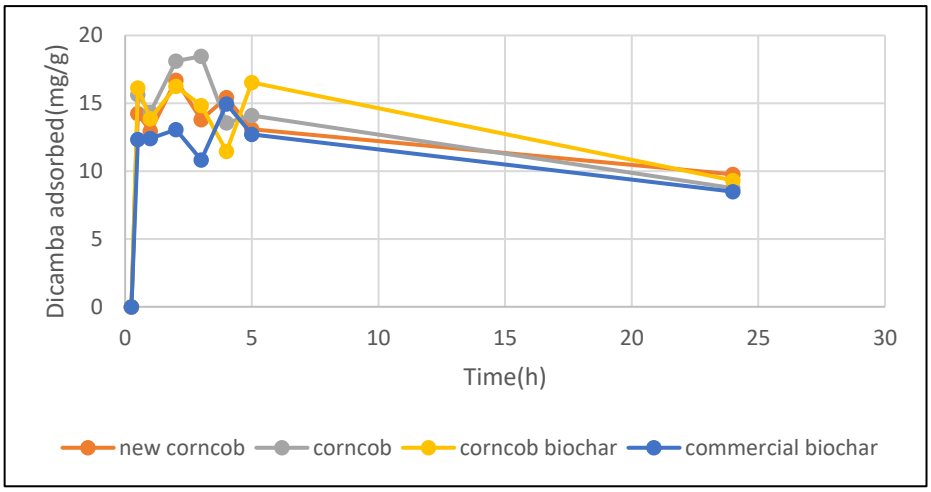

Figure 30 Kinetic adsorption of Dicamba on biochar, new biochar, corncob, and new corncob (average of 4 replicates ± standard deviation).

After the initial rapid phase, a small but noticeable decrease in adsorbed Dicamba mass was observed for all materials between 5 h and 24 h, possibly due to partial desorption. This phenomenon has been previously reported for weakly adsorbed organic compounds on lignocellulosic. The overall differences among materials were less pronounced compared to copper adsorption tests, indicating that Dicamba adsorption is less selective and more strongly governed by physical adsorption and surface affinity rather than specific binding to functional groups.

The kinetic adsorption data for Dicamba were fitted to three commonly used models: the pseudo-first-order, pseudo-second order, and Elovich models (Table 5). Among these, the pseudo-second-order model provided the best fit for all materials, as indicated by the highest R^2 values, which ranged from 0.966 for corncob to 0.9946 for new corncob. This suggests that Dicamba adsorption is likely governed by chemisorption mechanisms, involving valency forces through sharing or exchange of electrons between adsorbent and adsorbate.

For the pseudo-first-order model, only the corncob biochar and commercial biochar materials showed a computable fit, but with low R^2 values (0.735 and 0.1751, respectively), indicating that this model poorly represents the adsorption kinetics of Dicamba in these systems. The Elovich model, often used to describe heterogeneous adsorption surfaces, did not fit the data well in this study. The R^2 values were significantly lower for all tested materials, especially for commercial biochar and corncob, suggesting that this model is not suitable for capturing Dicamba adsorption behavior in the present systems.

Table 5 Kinetic model fitting parameters for Dicamba adsorption on Commercial biochar, corncob biochar, corncob, and new corncob

	Pseudo-first order model		
	k_1 (min^{-1})	q_e (mg/g)	R^2
New corncob	-	-	-
Corncob	-	-	-
Corncob biochar	0.04	0.09	0.73
Commercial biochar	0.01	0.08	0.17
	Pseudo-second order model		
	k_2 (mg/g min)	q_e (mg/g)	R^2
New corncob	4.88	12.4	0.99
Corncob	0.09	16.10	0.96
Corncob biochar	0.20	14.28	0.98
Commercial biochar	0.12	14.12	0.97
	Elovich model		
	a (mg/g)	b (mg/g min)	R^2
New corncob	$2.8.10^{+31}$	7.70	0.16
Corncob	$4.1.10^{+25}$	7.12	0.04
Corncob biochar	$2.1.10^{+21}$	9.65	0.11
Commercial biochar	$2.3.10^{+52}$	10.00	0.005

Overall, the pseudo-second-order model best describes the kinetics of Dicamba adsorption across all tested adsorbents, reinforcing the hypothesis that chemical interactions play a dominant role in the process. Notably, the highest k2 value (0.20988 mg/g·h) was observed for corncob biochar, followed closely by commercial biochar (0.12517 mg/g·h), reflecting their faster adsorption rates compared to new corncob and raw corncob.

3.3.4. Equilibrium adsorption (Dicamba)

3.3.4.1. Volume effect

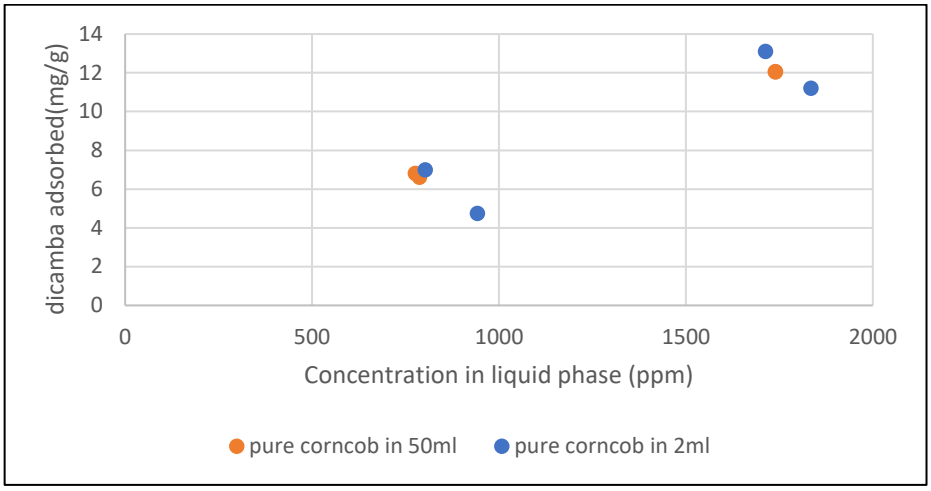

Figure 31 Effect of volume on Dicamba adsorption onto pure corncob

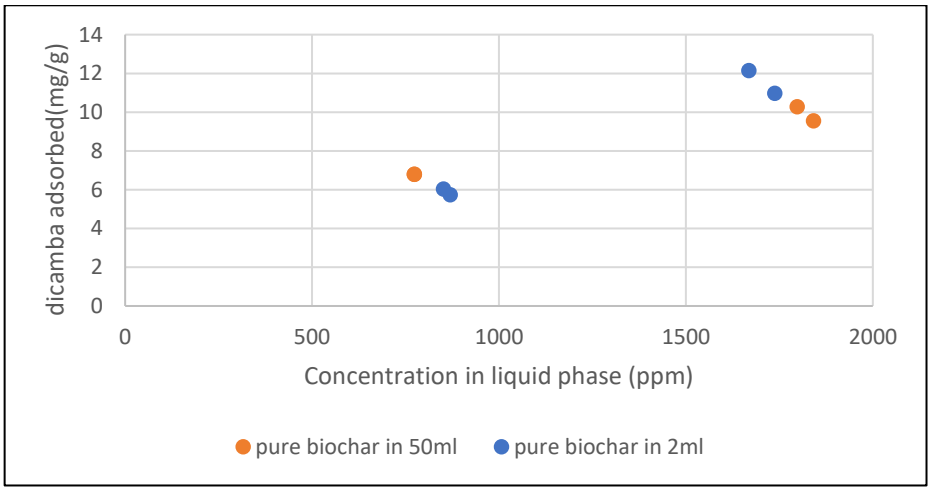

Figure 32 Effect of volume on Dicamba adsorption onto pure biochar

The effect of solution volume and adsorbent mass on Dicamba adsorption was evaluated by comparing batch tests performed in two configurations.

For pure corncob (Figure 31), no significant differences were observed between the adsorption curves obtained in the 2 mL and 50 mL tests. Adsorption capacities were consistent across the tested concentration range, confirming that under these conditions, Dicamba adsorption on corncob is not significantly affected by variations in solution volume or solid/liquid ratio. This is consistent with previous findings showing that Dicamba adsorption on lignocellulosic materials such as corncob is mainly governed by surface interactions, which are not strongly limited by diffusion or volume effects.

For pure biochar (Figure 32), a very similar behavior was observed. The adsorption curves in the 2 mL and 50 mL tests closely overlapped, indicating that biochar-based adsorption of Dicamba is also relatively unaffected by the changes in volume and adsorbent mass under the tested conditions

3.3.4.2. Comparison of all materials

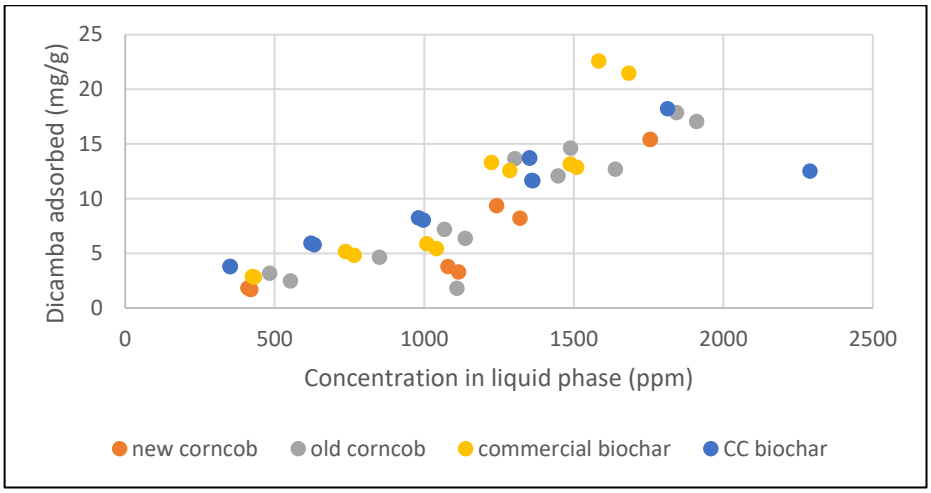

Figure 33 Comparison of Dicamba adsorption performance of new corncob, old corncob, new biochar, and commercial biochar.

Finally, a direct comparison was made between all tested materials to assess their overall Dicamba adsorption performance under equilibrium conditions. The results are reported in Figure 33.

Among the tested amendments, biochar showed the highest Dicamba adsorption capacity, reaching values up to 20–22 mg/g at the highest Dicamba concentrations tested. New biochar also exhibited good adsorption performance, although slightly lower than the commercial biochar, with capacities around 15–18 mg/g.

Old corncob and new corncob both exhibited similar Dicamba adsorption capacities, with maximum values around 15–18 mg/g, comparable to those of new biochar. Overall, the materials followed the following adsorption capacity trend:

Commercial biochar > New biochar ≈ Old corncob ≈ New corncob

These results indicate that both biochar-based and corncob-based materials provide comparable performance for Dicamba adsorption.

Table 6 Freundlich and Langmuir parameters obtained from Dicamba isotherm modelling

	Freundlich			Langmuir		
	1/n (-)	Kf ((mg/g)*(l/mg)$^{1/n}$)	R2 (-)	q max (mg/g)	L(l/g)	R2
CC biochar	0.92	1.49E-02	0.96	190.58	4.70E-05	0.99
New corncob	1.43	2.83E-04	0.85	22.03	1.75E-04	0.91
Corncob	1.47	2.32E-04	0.66	76.91	6.40E-05	0.42
Pure biochar	1.43	4.17E-04	0.89	27.58	2.13E-04	0.94

To better describe the adsorption equilibrium behavior of Dicamba on the tested amendments, the experimental data were fitted using both the Freundlich and Langmuir isotherm models. The corresponding fitting parameters are reported in Table 6.

Overall, the Langmuir model provided a good fit for new biochar ($R^2 = 0.99$) and new corncob ($R^2 = 0.91$), indicating that for these materials, Dicamba adsorption occurs mainly via monolayer adsorption on well-defined surface sites.

For pure biochar, both models provided a good fit ($R^2 = 0.94$ for Langmuir, 0.89 for Freundlich), suggesting a combination of monolayer and multilayer adsorption mechanisms, consistent with the complex surface heterogeneity of biochar.

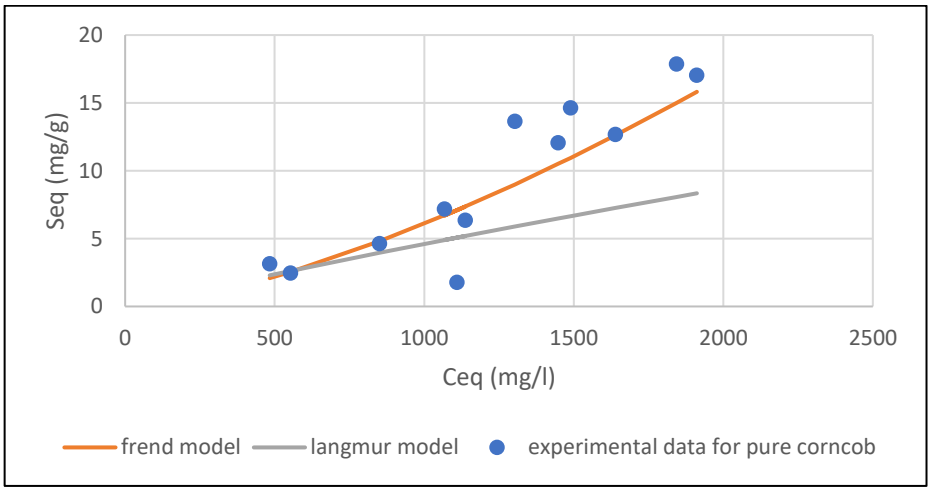

Figure 34 experimental data fitting with Freundlich (in orange) and Langmuir (in gray) model for corncob

In contrast, corncob exhibited a better fit with the Freundlich model ($R^2 = 0.66$ vs. 0.42 for Langmuir) in figure 34, suggesting that adsorption on corncob occurs on a heterogeneous surface with varying affinity sites, rather than through strictly monolayer adsorption.

The calculated q_{max} values highlight the different adsorption capacities of the materials:

- The new biochar exhibited the highest capacity (190.58 mg/g), confirming its strong potential for Dicamba adsorption.
- Pure corncob and new corncob exhibited lower but still significant capacities (76.91 mg/g and 22.03 mg/g, respectively).
- Pure biochar showed an intermediate capacity (27.58 mg/g), in line with the trends observed in the equilibrium curves (Section 3.3.4.2).

These results confirm that biochar-based materials exhibit superior adsorption capacities for Dicamba, likely due to a combination of hydrophobic interactions, hydrogen bonding, and surface heterogeneity. Corncob-based materials, while showing lower adsorption capacities, still offer promising performance, particularly when considering their availability and sustainability as agri-food waste products.

3.4. Column transport tests

3.4.1. Copper sulfate

The materials were packed with different bulk densities and porosities, which influenced their flow dynamics. Notably, the sand–biochar columns had shorter lengths and lower biochar content compared to the sand–corncob setups, yet they required longer injection durations, up to 40 hours, due to slower flow and higher retention. This contrasts with the 25-hour injection time needed for sand and corncob mixtures. Overall, biochar-amended columns showed lower hydraulic conductivity and dispersivity, supporting their stronger retention behavior during contaminant transport.

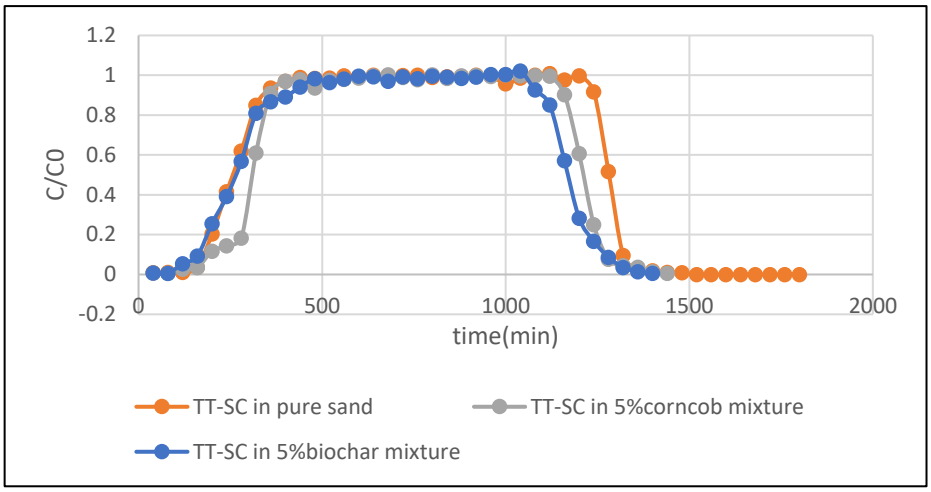

Figure 35 BTC tracer tests in saturated conditions in different materials

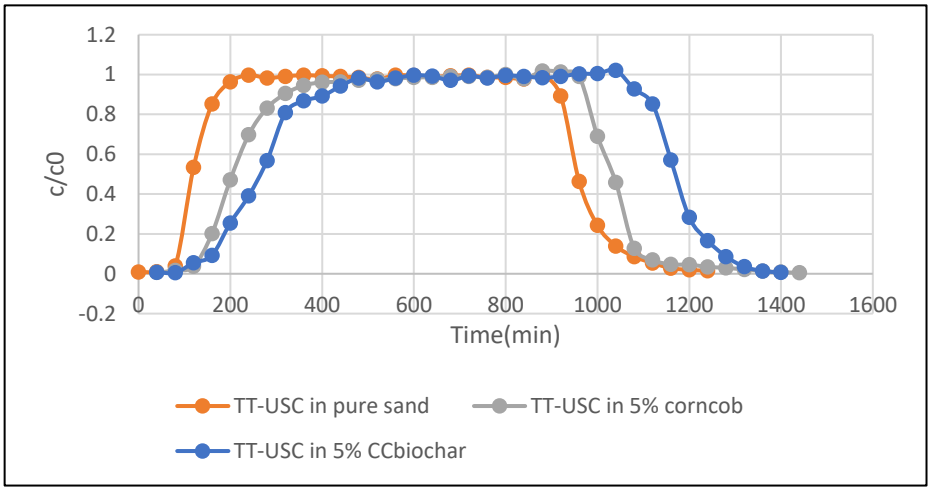

Figure 36 BTC tracer tests in unsaturated conditions in different materials

The breakthrough curves (BTCs) for tracer tests conducted under saturated and unsaturated conditions are shown in Figures 35 and 36, respectively, in columns filled with pure sand and sand amended with 5% corncob or biochar. In these plots, the time axis starts at the moment the tracer was injected, ensuring a consistent comparison of the rising front of the BTCs across all materials. Under saturated conditions (Figure 35), the rising edges of the BTCs appear at different times, indicating variation in the porosity of the materials. The earlier breakthrough observed in pure sand suggests lower retention and faster flow, while the delayed peaks in the corncob and biochar-amended columns indicate greater porosity or higher dispersion, which should be confirmed by porosity calculation using tracer fitting. A similar trend is visible under unsaturated conditions (Figure 36), although the broader tails and slower rising fronts reflect

the influence of lower water content and increased interaction between the tracer and solid phase. Again, pure sand shows the fastest response, while the amendments cause a delayed and more dispersed tracer transport, which points to possible differences in water retention or immobile zones created by the organic additives. To support clarity, the term "Tracer Test-Saturated Condition" has been abbreviated to "TT-SC" and "Tracer Test-Unsaturated Condition" to "TT-USC," defined accordingly.

Table 7 Duration of injection steps (hours) for saturated tracer (TT-SC), unsaturated tracer (TT-USC), and copper solution in different column setups.

	TT-SC duration(h)	TT-USC duration(h)	Copper injection(h)
Pure sand	17	15	18
5% new corncob	16	14	24.5
5% CC biochar	16.5	16.5	40h

To account for the differences in flow and retention characteristics among the tested materials, the duration of each injection step, saturated tracer (TT-SC), unsaturated tracer (TT-USC), and copper solution, was adjusted accordingly. Table 7 reports the total duration of each step for the different column setups, ensuring that each test reached a stable and complete breakthrough curve.

The rising portion of the breakthrough curves for copper injection in the three column setups (Figures 37–39) highlights the combined effects of adsorption behavior and differences in injection duration. In the pure sand column, the copper curve rose quickly, reaching the C/C_0 midpoint at approximately 156 minutes. This early breakthrough aligns with the short injection time (18 hours) and reflects the inert nature of sand, which led to limited interaction with the solute. The high mass balance (94%) confirms that most of the copper passed through the column with minimal retention. In the sand + 5% corncob column, the rise of the copper curve was delayed, with the midpoint occurring at 637.75 minutes. This shift corresponds to a longer injection duration (24.5 hours) and suggests increased interaction with the porous matrix. The mass balance was reduced to 78%, indicating partial retention of copper due to the presence of organic functional groups in corncob. In the sand + 5% biochar column, the breakthrough was significantly delayed, with the midpoint only reached after 1196.45 minutes. This delay is partly due to the extended injection time (40 hours), but also highlights the strong retention properties of biochar. The lowest mass balance (57.7%) in this case confirms substantial copper adsorption. While the breakthrough delays follow the order sand < corncob < biochar, these shifts are also influenced by the differing durations and pore volumes. Therefore, direct

comparison of copper and tracer curves within each column remains the most reliable indicator of retention efficiency.

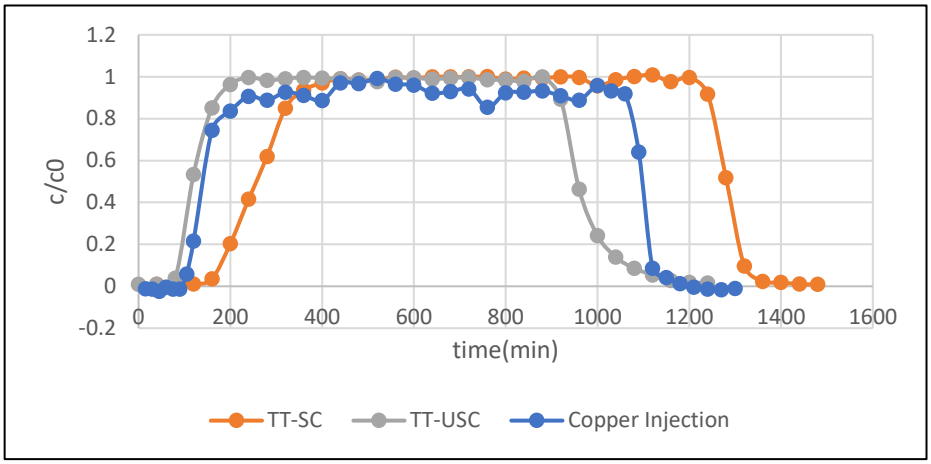

Figure 37 BTC column pure sand with copper

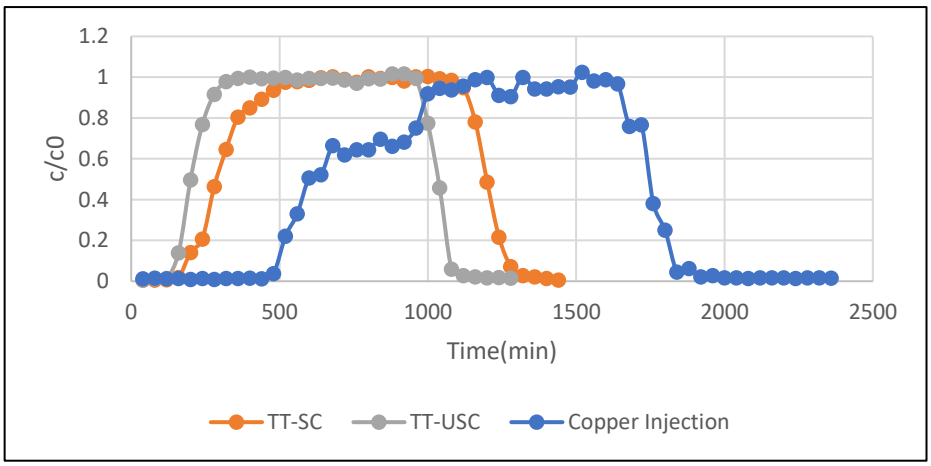

Figure 38 BTC column sand+5% new corncob with copper

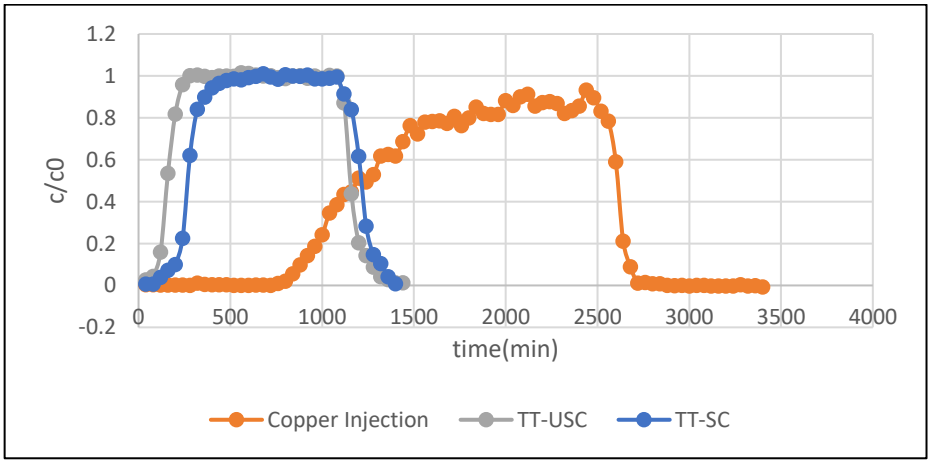

Figure 39 BTC column sand+5% CC biochar with copper

3.4.2. Dicamba

The tracer tests conducted under saturated and unsaturated conditions for the three column setups (pure sand, sand + 5% corncob, and sand + 5% biochar) were previously discussed and are not repeated here for Dicamba injections. Since the same column configurations, porosities, and water contents were used for both copper and Dicamba tests, the flow characteristics established through tracer breakthrough curves remain valid. The durations of injection steps specific to Dicamba experiments are summarized in Table 8, ensuring comparability across materials.

Table 8 Duration of injection steps (hours) for saturated tracer (TT-SC), unsaturated tracer (TT-USC), and Dicamba solution in different column setups.

	TT-SC duration(h)	TT-USC duration(h)	Copper injection(h)
Pure sand	17	15	15
5% new corncob	16	14	24.08
5% CC biochar	16.5	16.5	39.5h

The BTCs obtained for Dicamba in the different column setups are reported in Figures 40–42. In the pure sand column (Figure 40), Dicamba showed an early breakthrough, with the C/C_0 midpoint reached at 197.75 minutes. The BTC was sharp and symmetrical, and the mass balance was 99.74%, indicating almost complete recovery and confirming the high mobility of Dicamba in the inert sandy matrix.

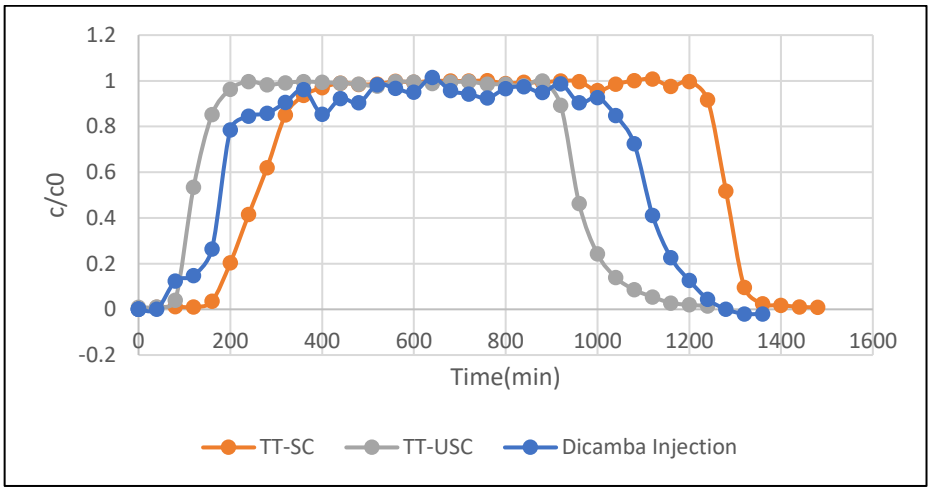

Figure 40 BTC column pure sand with dicamba

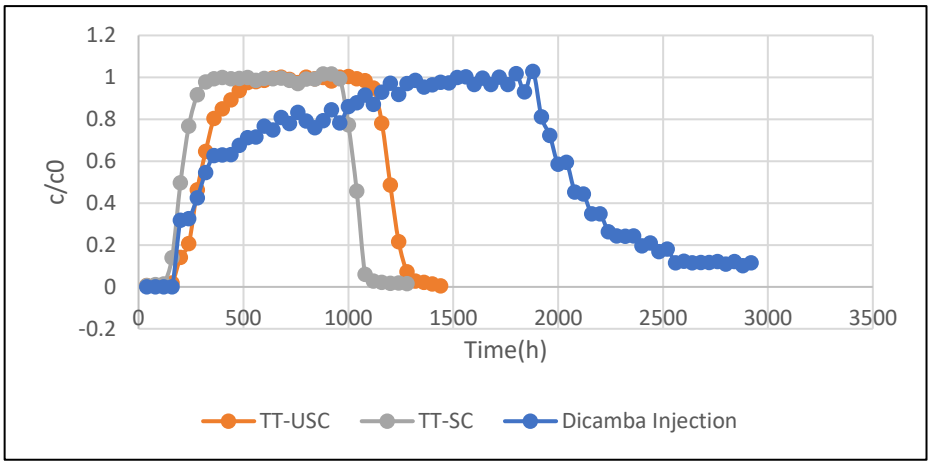

Figure 41 BTC column sand+5%corncob with dicamba

In the column packed with sand + 5% corncob (Figure 41), Dicamba exhibited a slightly delayed breakthrough, with the midpoint reached at 357.75 minutes. The BTC also showed slight tailing, and the mass balance was 108.53%. The delayed breakthrough occurred 200 minutes later and still indicates an enhanced retention of Dicamba in the presence of corncob. This behavior is attributed to the presence of organic matter in corncob, providing additional adsorption sites for weakly polar compounds such as Dicamba.

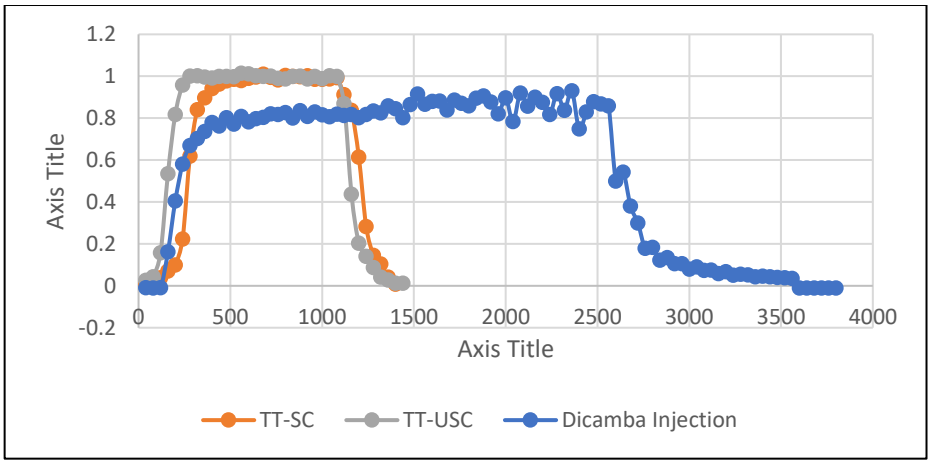

Figure 42 BTC column sand+5%CC biochar with dicamba

In the column packed with sand + 5% biochar (Figure 42), the breakthrough of Dicamba occurred with moderate tailing after 40 hours of injection. The midpoint was reached at 196.45 minutes, and the mass balance was 90%. This is consistent with the different adsorption mechanisms governing the interaction of polar organic compounds with biochar surfaces, which may not provide as high an affinity for Dicamba as for metal cations.

Overall, the column tests confirmed that Dicamba exhibited high mobility in pure sand, and the presence of corncob enhanced Dicamba retention and delayed breakthrough.

These findings align with the batch adsorption results and highlight the different behaviors of Copper and Dicamba in porous media, as governed by their respective interaction mechanisms with natural amendments.

Table 9 characteristics of column transport tests: geometrical parameters and mass balance results.

CuSO4			
	sand	**Sand+5% corncob**	**Sand+5% CC biochar**
Column length (cm)	16.5	19	15
Bulk density (g/cm3)	1.55	1.26	1.28
Pore volume time(min) Saturated condition	278	317	276
Pore volume time(min), Unsaturated condition	116	197.75	156.45
C/C_0 Plateau	1	0.99	0.91
Time to C/C_0=0.5 (min)	156.43	637.75	1197
Percentage of CuSO4 out (%)	94	78	57
Dicamba			
Column length (cm)	16	19	15
Bulk density (g/cm3)	1.55	1.25	1.28
Pore volume time(min) Saturated condition	278	317	276
Pore volume time(min), Unsaturated condition	118	197.75	156.45
C/C_0 Plateau	1	0.99	0.92
Time to C/C_0=0.5 (min)	197.75	360	197
Percentage of Dicamba out (%)	113	110	89

Table 9 summarizes the key geometrical and transport parameters obtained from the column experiments for both $CuSO_4$ and Dicamba. For copper, the time to reach $C/C_0 = 0.5$ increased significantly from sand (156.43 min) to corncob (637.75 min) and biochar (1197 min), highlighting the enhanced retention capacity of the organic amendments, as it was shown in the breakthrough curves. A similar trend, though less pronounced, was observed for Dicamba, with time to $C/C_0 = 0.5$ rising from 197.75 min in sand to 360 min and 197 min in corncob and biochar columns, respectively. Overall, the table confirms the stronger retention of copper compared to Dicamba and highlights the influence of adsorbent type on transport behavior in porous media.

3.4.3. Hydrus 1D

The breakthrough curves obtained from the column experiments were interpreted using the numerical model HYDRUS 1D (Šimůnek, 2013), which solves the advection–dispersion equation under variably saturated conditions. A two-site sorption model was adopted, described by a system of equations that distinguishes between instantaneous and kinetic adsorption mechanisms. In the case of the non-reactive tracer (KBr), transport was modeled by solving the classical advection–dispersion equation under variably saturated conditions, neglecting any sorption terms. The governing equation is:

$$\frac{\partial \theta c}{\partial t} = \frac{\partial}{\partial z}(\theta D \frac{\partial c}{\partial z}) - \frac{\partial qc}{\partial z} + \varphi \qquad \text{eq12}$$

where θ is the volumetric water content [L^3/L^3], c is the solute concentration in the aqueous phase [M/L^3], q is the Darcy flux [L/T], D is the hydrodynamic dispersion coefficient [L^2/T], and φ is a sink term that can account for chemical degradation or other losses.

For reactive solutes such as copper and dicamba, a two-site sorption model was adopted:

$$\frac{\partial \theta c}{\partial t} + \rho \frac{\partial s_e}{\partial t} + \rho \frac{\partial s_k}{\partial t} = \frac{\partial}{\partial z}(\theta D \frac{\partial c}{\partial z}) - \frac{\partial qc}{\partial z} + \varphi \qquad \text{eq13}$$

In this equation, ρ is the bulk density of the medium [M/L^3], and s_e and $s_k$represent the mass of solute adsorbed onto instantaneous and kinetic sorption sites, respectively, expressed in [M/M]. The equilibrium sorption (type-1) is described as:

$$s^e = f_e . F(c) \qquad \text{eq14}$$

where f_e is the fraction of sorption sites assumed to be in equilibrium with the liquid phase, and $F(c)$ is the adsorption isotherm (typically linear, Langmuir, or

Freundlich). The kinetic sorption (type-2), associated with slower mass transfer between phases, is governed by:

$$\rho \frac{\partial s_k}{\partial t} = \alpha_k \rho (s_k^e - s_k) + \varphi_k \qquad \text{eq15}$$

where α_k is the first-order kinetic rate constant [T^{-1}], s_k is the equilibrium concentration at the kinetic sorption site [M/M], and $\varphi_k$is a sink/source term. The kinetic equilibrium concentration is given by:

$$s_e^k = (1 - f_e).K_d.c \qquad \text{eq16}$$

where K_d is the linear distribution coefficient [L^3/M]. While these equations assume linear sorption behavior, HYDRUS also allows for modeling non-linear sorption. In this case, the general form of the sorption isotherm is:

$$s = \frac{K_s c^\beta}{1 + \eta c^\beta} \qquad \text{eq17}$$

where β is a dimensionless exponent and η is the nonlinearity parameter. When η=0, the model simplifies to the Freundlich isotherm, while η =1 corresponds to the Langmuir model.

For each column test, the parameters fitted included the distribution coefficient K_d, and, in the case of copper, the kinetic rate constants were relevant. Fixed parameters, such as porosity (θ), bulk density (ρ), and column dimensions, were experimentally determined and kept constant during model calibration. For the non-reactive tracer tests, only dispersivity was fitted, while sorption terms were neglected. In Figure 43, an example of least square fitted parameters in Hydrus for copper adsorption by a column with sand+5% cc biochar is shown.

```
Non-linear least-squares analysis: final results
================================================
                                        95% Confidence limits
Variable        Value        S.E.Coeff.     Lower         Upper
  FRAC     0.29694E-01    0.75247E-03  0.28196E-01  0.31191E-01
  KD       0.16154E-02    0.54035E-04  0.15079E-02  0.17230E-02
  BETA     0.49173E-02    0.77989E-04  0.47621E-02  0.50725E-02
  SNKL1    0.12258E-02    0.46151E-04  0.11339E-02  0.13176E-02
  ALPHA    0.46580E-02    0.95865E-04  0.44672E-02  0.48488E-02


Contributions to the final objective function

Measurement Set   4:   0.3940E-01

RSQUARE for regression of predicted vs observed =0.96228
```

Figure 43 example of least square fitted parameters in Hydrus for copper adsorption by column with sand+5% cc biochar

The BTCs of both Copper and Dicamba were fitted using this modeling approach by adjusting parameters such as the distribution coefficient K_d. In particular, the application of the two-site model proved essential for simulating the pronounced tailing observed in the Copper BTCs for the biochar-amended columns, where strong retention and slow desorption were evident. On the other hand, the breakthrough curves for Dicamba were more symmetrical and consistent with equilibrium-dominated sorption behavior, especially in the sand and sand–corncob columns.

Model calibration was performed by minimizing the root mean square error (RMSE) between measured and simulated concentrations. The fitted curves and HYDRUS output parameters are reported in Figure 44. Overall, the simulation confirmed the stronger retention of copper in biochar, moderate retention in corncob, and limited interaction in pure sand. For Dicamba, retention was generally weaker but still influenced by the presence of organic matter in the corncob and biochar mixtures.

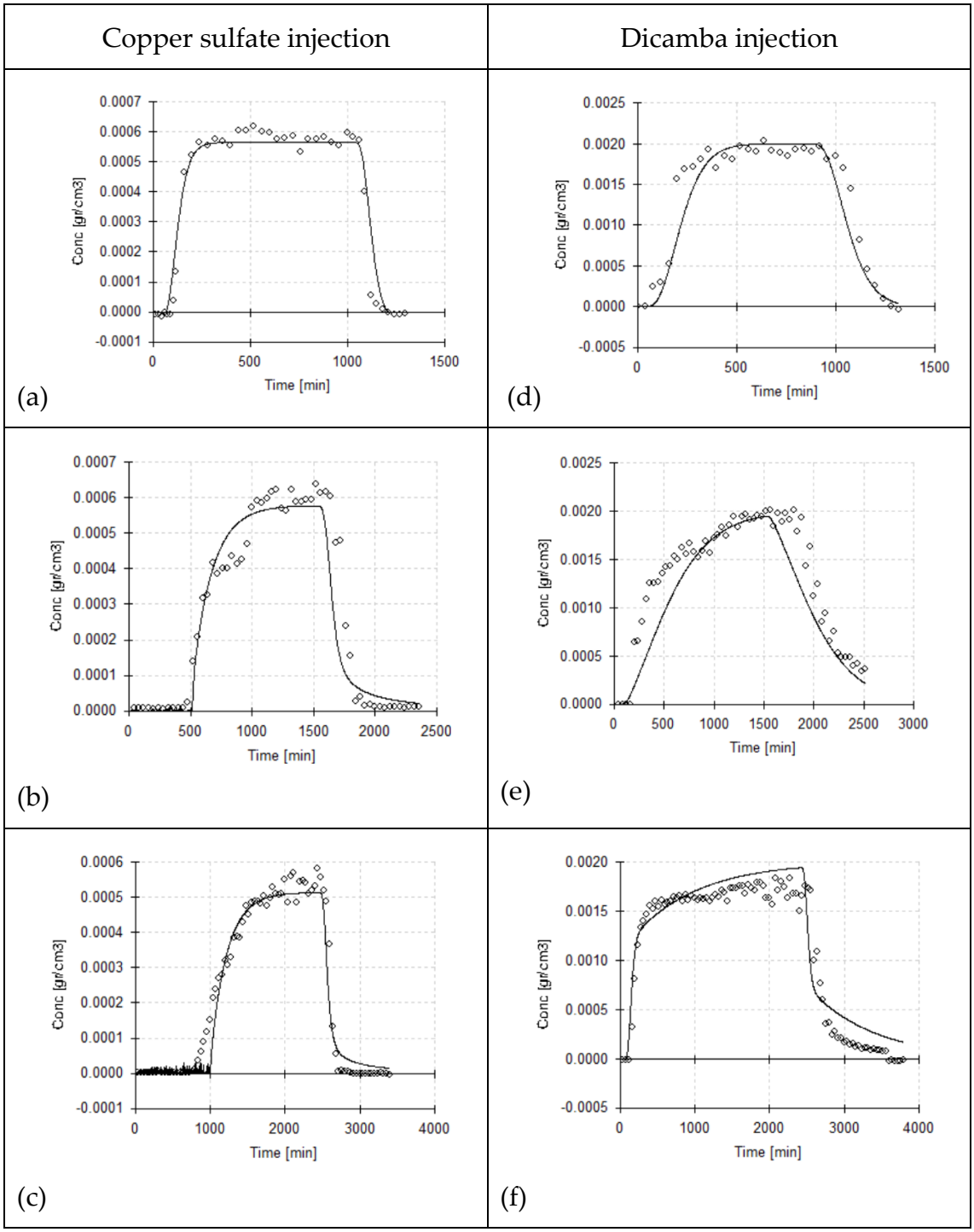

Figure 44 experimental (points) and modelled (line) breakthrough curve for sand and sand-amendment ((a)pure sand, (b)sand and corncob mixture, (c)sand and biochar mixture, (d)pure sand, (e)sand and corncob mixture, (f)sand and biochar mixture)

The physical properties of the columns, including column dimensions, pore volumes (PV), and volumetric water content, were determined from tracer tests under saturated and unsaturated conditions. Table 10 summarizes these values for all column setups obtained by Hydrus 1D with all of which have an R^2>0.9.

Table 10 Column transport tests: hydrodynamic parameters obtained by Hydrus for copper and Dicamba injection

Cuso4			
	sand	**Sand+5% corncob**	**Sand+5% CC biochar**
Porosity (-)	0.43	0.43	0.53
Unsaturated water content (cm3/cm3)	0.21	0.29	0.29
Saturated hydraulic conductivity Ks (cm/min)	0.33	0.087	0.25
Dispersivity (cm)	0.7	0.51	0.55
Adsorption isotherm coefficient Kd (l/g)	8.20×10^{-05}	5.98×10^{-07}	1.60×10^{-06}
Dicamba			
Porosity (-)	0.43	0.45	0.48
Unsaturated water content (cm3/cm3)	0.17	0.31	0.29
Saturated hydraulic conductivity Ks (cm/min)	0.5	0.060	0.24
Dispersivity (cm)	0.73	1.09	0.55
Adsorption isotherm coefficient Kd (l/g)	1.20×10^{-04}	4.30×10^{-04}	4.60×10^{-04}

The values of K_d derived from Hydrus modeling reflect distinct sorption behaviors between copper and Dicamba across the tested materials. For copper, the lowest K_d was found in the corncob-amended column, indicating limited retention, while the highest value was observed in the pure sand column. In contrast, Dicamba showed consistently higher K_d values, suggesting stronger interaction with the solid phase across all columns, with the biochar-amended column exhibiting the highest value.

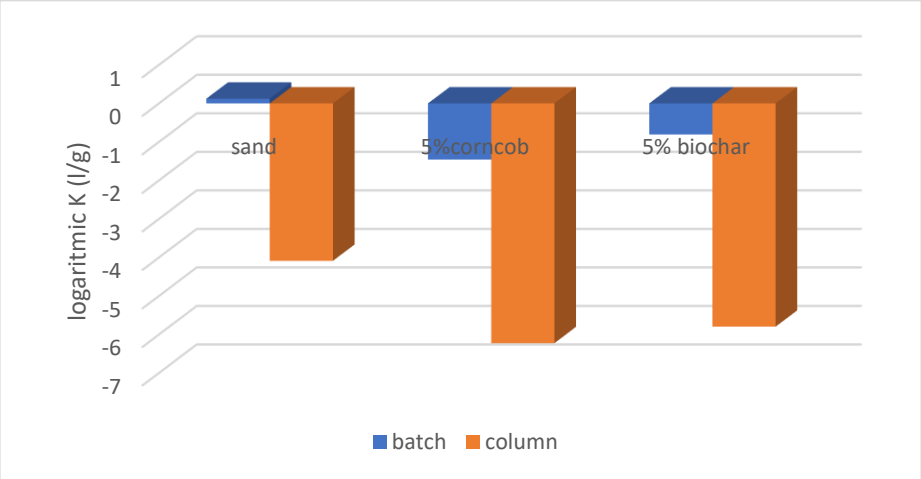

Figure 45 Comparison of Kd from column and Kf from batch test on copper adsorption

For a better comparison of what we have done in the series of experiments, both in batch and column tests, figure 45 presents a comparison between the distribution coefficient (K_d) obtained from column modeling in Hydrus 1D and the Freundlich coefficient (K_f) derived from batch isotherm fitting for copper adsorption. To facilitate visualization, the values are shown on a logarithmic scale. Despite the difference in test types and modeling approaches, both parameters display a consistent trend across materials: the highest sorption is observed for sand, followed by 5% CC biochar and then 5% corncob. This agreement confirms that, although absolute values differ due to experimental conditions, the relative sorption capacities remain consistent between batch and column experiments.

Overall, the agreement between batch and column trends reinforces the reliability of both approaches in evaluating sorption behavior under different experimental conditions.

4 Conclusion

This study investigates the role of agri-food waste materials, both in raw and processed conditions, in particular raw corncob and pyrolyzed biochar, in limiting the environmental spread of agrochemicals such as copper and Dicamba through adsorption mechanisms. The main goal was to evaluate their performance through detailed material characterization, batch equilibrium studies, and column transport tests.

The results illustrated that pure biochar consistently exhibited the highest adsorption capacity for both copper and Dicamba, followed by corncob biochar and raw corncob. Material properties such as pH, EC, and bulk density varied notably across samples, which influences their performance. Adsorption isotherms fitted using Langmuir and Freundlich models showed that raw corncob generally followed Langmuir behavior, suggesting monolayer adsorption, whereas biochar showed a better fit with the Freundlich model, indicating adsorption on heterogeneous surfaces.

Kinetic studies further supported these trends, showing faster adsorption for copper than for Dicamba, and the time needed for equilibrium adsorption tests. While increasing biochar or corncob content improved performance, the effectiveness of mixtures was reduced due to the dilution effect of sand.

Column transport tests were performed to study the effect of the different amendments in hydrodynamic conditions. The results confirmed the higher affinity of biochar for copper sulphate, with almost half of the copper exiting from the column during the tests, compared to sand and sand-corncob columns.

Despite the promising results, some limitations still exist. The tests were done on a small scale, the size of the adsorbent particles was not measured to see the possible impact, and the column setup was a simplified version of real conditions. Further investigations under field-scale scenarios are essential to validate the applicability of these materials.

In conclusion, this research confirms that biochar and corncob, as agri-food wastes, can be used both to improve the physical chemical characteristics of the soil, as already done sometimes in current agronomic practices, but also to increase the adsorption of pesticides in the soil, thus limiting the spreading of

both diffuse and local contaminations generated in an agricultural context. These are low-cost and sustainable solutions to mitigate agrochemical leaching in soil and groundwater. Their valorization aligns with the principles of circular economy and contributes to several Sustainable Development Goals (SDGs), especially those related to clean water, responsible production, and climate action.

5 Bibliography

(EEA). (2018). *Soil pollution and ecosystems*. Retrieved from European Environment Agency: https://www.eea.europa.eu/publications/zero-pollution/ecosystems/soil-pollution

(EEA). (2022). *Europe's groundwater — a key resource under pressure.* Copenhagen: European Environment Agency,Briefing no. 03/2022. ISBN: 978-92-9480-460-0 - ISSN: 2467-3196. doi:https://doi.org/10.2800/629513

(EPA). (2017). *Pesticide product label: Dicamba 49.8% SL.* U.S. Environmental Protection Agency,EPA Reg. Number: 85678-47. Retrieved from https://www3.epa.gov/pesticides/chem_search/ppls/085678-00047-20170927.pdf

(FAO). (2013). *Food Wastage Footprint: Impacts on Natural Resources.* Food and Agriculture Organization of the united nations, ISBN 978-92-5-107752-8. Retrieved from https://www.fao.org/3/i3347e/i3347e.pdf

(FAO). (2020). *International Year of Plant Health.* Rome: Food and Agriculture Organization of the united nations,ISBN 978-92-5-135056-0. doi:https://doi.org/10.4060/cb7056en

(MDA). (2019). *Dicamba*. Retrieved from Minnesota Department of Agriculture: https://www.mda.state.mn.us/dicamba

(USGS). (2022). *Pesticides and water quality*. Retrieved from U.S. Geological Survey: https://www.usgs.gov/special-topics/water-science-school/science/pesticides-and-water-quality

Agegnehu, G. N. (2016). The effects of biochar, compost and their mixture on soil properties and crop yield: A review. *Science of the Total Environment*, 295–301. doi:10.1016/j.scitotenv.2015.11.054

Aguiar, A. C. (2023). Sorption, leaching, and degradation of dicamba in two Brazilian soils: A study into soil layers. *Crop Protection*, 106393. doi:10.1016/j.cropro.2023.106393

Ahemad, M. (2013). Pesticides as Antagonists of Rhizobia and the Legume-Rhizobium Symbiosis: a Paradigmatic and Mechanistic Outlook. *Biochemistry & Molecular Biology*, 65–75. doi:10.12966/bmb.12.02.2013

Ahmad, M. R. (2014). Biochar as a sorbent for contaminant management in soil and water: a review. *Chemosphere, 99*, 19–33. doi:10.1016/j.chemosphere.2013.10.071

Ahmed, e. a. (2023). Recent progress on corn (Zea mays L.)-based materials as raw, chemically modified, carbonaceous, and composite adsorbents. *Environmental Chemistry Letters (assumed, per style of broader review)*. doi: 10.1016/j.jaap.2023.106004

Aldrich, A. P. (2002). Speciation of Cu and Zn in drainage water from agricultural soils. *Environmental Science & Technology*, 4824–4830. doi:https://doi.org/10.1021/es020045s

Bakshi, S. Z. (2014). Biochar amendment affects leaching potential of copper and nutrient release behavior in contaminated sandy soils. *Journal of Environmental Quality, 43*, 1894–1903. doi:https://doi.org/10.2134/jeq2014.05.0213.

Beryani, A. B. (2022). Exploring the potential of graphene oxide nanosheets for porous media decontamination from cationic dyes. *Journal of Hazardous Materials*, Article 127468. doi:https://doi.org/10.1016/j.jhazmat.2021.127468.

Buasri, A. C. (2023). Equilibrium and kinetic studies of biosorption of Zn(II) ions from wastewater using modified corncob. *APCBEE Procedia*, 60–64. doi:https://doi.org/10.1016/j.apcbee.2012.06.046

Cao, X. M. (2011). Simultaneous immobilization of lead and atrazine in contaminated soils using dairy-manure biochar. *Environmental Science & Technology*, 4884–4889. doi:https://doi.org/10.1021/es103752u

Cara, I. Ț. (2022). Biochar: A Promising Strategy for Pesticide-Contaminated Soils. *Agriculture*, 1579. doi: https://doi.org/10.3390/agriculture12101579

Carvalho, F. (2017). Pesticides, Environment, and Food Safety. *Food and Energy Security, 6(2)*, 21–32. doi:10.1002/fes3.108

Cataldo, A. D. (2021). Adsorption of pesticides on biochar: A review. *Environmental Science and Pollution Research, 28(5)*, 1–15. doi:10.1007/s11356-021-12345-6

Chaudhari, V. &. (2022). Removal of nickel from aqueous solution by using corncob as adsorbent. *Materials Today: Proceedings, 61 Part 2*, 307–314. doi:10.1016/j.matpr.2021.09.458

Chen, Y. F. (2022). Polyethyleneimine-modified corncob magnetic gel composite for efficient removal of Cu(II) from aqueous solution. *RSC Advances*, 3744–3757. doi:10.1039/D1RA08699E

Dey, T. B. (2021). Valorization of agro-waste into value added products for sustainable development. *Bioresource Technology Reports*, Article 100834. doi:10.1016/j.biteb.2021.100834

Diacono, M. &. (2010). Long-term effects of organic amendments on soil fertility: a review. *Agronomy for Sustainable Development, 30*, 401–422. doi: 10.1051/agro/2009040

Dordio, A. &. (2013). Organic xenobiotics removal in constructed wetlands, with emphasis on the importance of the support matrix. *Journal of Hazardous Materials, 252–253*, 272–292. doi:10.1016/j.jhazmat.2013.03.008

Escudero-Curiel, S. C. (2023). From Waste to Resource: Valorization of Lignocellulosic Agri-Food Residues through Engineered Hydrochar and Biochar for Environmental and Clean Energy Applications—A Comprehensive Review. *foods*, Article 3646. doi:10.3390/foods12193646

Fucic, A. D. (2021). Reproductive health risks associated with occupational and environmental exposure to pesticides. *International Journal of Environmental Research and Public Health, 18(12)*, 6576. doi: 10.3390/ijerph18126576

Gani, A. A. (2023). Proximate and ultimate analysis of corncob biomass waste as raw material for biocoke fuel production. *Case Studies in Chemical and Environmental Engineering*, 100525. doi:https://doi.org/10.1016/j.cscee.2023.100525

Ge, L. Z. (2024). Comprehensive Review of Biomass Pyrolysis: Conventional and Advanced Technologies. *Energies, 17(20)*, 5082. doi:10.3390/en17205082

Ghasemi, J. A. (2003). Simultaneous determination of copper, nickel, cobalt and zinc using Zincon as a metallochromic indicator with partial least squares. *Analytica Chimica Acta*, 181–188. doi:8. https://doi.org/10.1016/s0003-2670(03)

Ghosh, U. Z. (2011). In-situ sorbent amendments: a new direction in contaminated sediment remediation. *Environmental Science & Technology, 45(1)*, 448–455. doi:10.1021/es102694h

Giambò, F., Teodoro, M., Costa, C., & Fenga, C. (2021). Toxicology and Microbiota: How Do Pesticides Influence Gut Microbiota? A Review. *International Journal of Environmental Research and Public Health*. doi:10.3390/ijerph18115510

Gomes, S. I., Scott-Fordsmand, J. J., Campos, E. V., Grillo, R., Fraceto, L. F., & Amorim, M. J. (2019). On the safety of nanoformulations to non-target soil invertebrates – an atrazine case study. *Environmental Science: Nano*, 1950–1958. doi:doi.org/10.1039/C9EN00242A

Gotore, O., Itayama, T., Dang, B., Nguyen, T., Ramaraj, R., Nakagoe, O., . . . Maseda, H. (2022). Adsorption analysis of ciprofloxacin and delafloxacin onto the corn cob derived-biochar under different pyrolysis conditions. *Biomass Conversion and Biorefinery*, 10373–10388. doi:https://doi.org/10.1007/s13399-022-03156-y

Granetto, M. B. (2024). The role of soil amendments in limiting the leaching of agrochemicals: Laboratory assessment for copper sulphate and dicamba. *Journal of Cleaner Production, 474*. doi:DOI: 10.1016/j.jclepro.2024.143532

Granetto, M. S. (2022). Natural clay and biopolymer-based nanopesticides to control the environmental spread of a soluble herbicide. *Science of the Total Environment*. doi: 10.1016/j.scitotenv.2021.151199

Ho, Y. &. (1999). Pseudo-second order model for sorption processes. *Process Biochemistry*, 451–465. doi:https://doi.org/10.1016/S0032-9592(98)00112-5

Kah, M. &. (2014). Nanopesticide research: Current trends and future priorities. *Environment International, 63*, 224–235. doi:https://doi.org/10.1016/j.envint.2013.11.015

Kajjumba, G. E. (2018). Modelling of Adsorption Kinetic Processes—Errors, Theory and Application. In *Advanced Sorption Process Applications.* Rijeka: IntechOpen. doi:https://doi.org/10.5772/intechopen.80495

Kan, T. S. (2016). Lignocellulosic biomass pyrolysis: A review of product properties and effects of pyrolysis parameters. *Renewable and Sustainable Energy Reviews, 57*, 1126–1140. doi:https://doi.org/10.1016/j.rser.2015.12.185

Kookana, R. S. (2011). Chapter three – Biochar application to soil: agronomic and environmental benefits and unintended consequences. In *Advances in Agronomy* (Vol. 40(3), pp. 1068–1080). Academic Press. doi: https://doi.org/10.1016/B978-0-12-385538-1.00003-2

Kori, R. S. (2018). Neurochemical and behavioral dysfunctions in pesticide-exposed farmworkers: A clinical outcome. *Indian Journal of Clinical Biochemistry*, 372–381. doi: https://doi.org/10.1007/s12291-018-0791-5

Lamichhane, J. R. (2017). Pesticide use and risk reduction in European farming systems with IPM: An introduction to the special issue. *Crop Protection, 97*, 1–6. doi:10.1016/j.cropro.2017.01.017

Lehmann, J. &. (2015). *Biochar for environmental management: Science, technology and implementation.* Routledge.

Lestari, A. C. (2020). Magnetically Modified Corn Cob as a New Low-Cost Biosorbent for Removal of Cu(II) and Zn(II) from Wastewater. *Jurnal Bahan Alam Terbarukan (JBAT)*, 96–102. doi:10.15294/jbat.v9i02.27136

Liu, Z. D. (2017). Biochar particle size, shape, and porosity act together to influence soil water properties. *PLoS ONE, 245*, e0179079. doi:https://doi.org/10.1371/journal.pone.0179079

Magdalena Joka Yildiz, M. K.-W. (2023). A Short Overview of the Possibilities of Using Waste from the Agri-Food Industry. *Advances in Science and Technology Research Journal, 27(1)*, 342–352. doi:10.12913/22998624/161840

Mahdi, Z. Y. (2018). Investigation of the kinetics and mechanisms of nickel and copper ions adsorption from aqueous solutions by date seed derived biochar. *Journal of Environmental Chemical Engineering*, 1171–1181. doi:https://doi.org/10.1016/j.jece.2018.01.021

Murtaza, G. J.-u.-R. (2021). Biochar for the management of nutrients and potentially toxic elements in soil. *Environmental Science and Pollution Research*, 9690–9708. doi:10.1007/s42729-021-00514-z

Nasiruddin Khan, M. &. (2007). Characterization of chemically modified corncobs and its application in the removal of metal ions from aqueous solution. *Journal of Hazardous Materials, 141(1)*, 237–244. doi:10.1016/j.jhazmat.2006.06.119

Paulauskas, R. P. (2024). erformance of Corn Cob Combustion in a Low-Temperature Fluidized Bed. *Energies, 17(9)*, 2196. doi: https://doi.org/10.3390/en17092196

Pérez-Lucas, G. V. (2018). Environmental Risk of Groundwater Pollution by Pesticide Leaching through the Soil Profile. Pesticides, Anthropogenic Activities and the Health of our Environment. doi:a. https://doi.org/10.5772/intechopen.82418

Pradhan, S. M.-A. (2022). Biochar from food waste: a sustainable amendment to reduce water stress and improve the growth of chickpea plants. *Biomass Conversion and Biorefinery, 12(3)*, 4549–4562. doi:10.1007/s13399-022-02575-1

Revellame, E. F. (2020). Adsorption kinetic modeling using pseudo-first order and pseudo-second order rate laws: A review. *Cleaner Engineering and Technology*, Article 100032. doi:https://doi.org/10.1016/j.clet.2020.100032

Saadi, M. E. (2024). Conversion of Waste Corn Cob to Highly Green Surface Activated Carbon. *Majalleh-ye Danishgahi (University Scientific Journal)*, 1139.

Schmidt, H.-P. (2015). *European Biochar Certificate (EBC) – Guidelines Version 6.1.* European Biochar Foundation. doi: https://doi.org/10.13140/RG.2.1.4658.7043

Sethi, R. D. (2019). *Groundwater engineering: A technical approach to hydrogeology, contaminant transport and groundwater remediation.* Springer. doi: https://doi.org/10.1007/978-3-030-20516-4

Shakya, A. &. (2023). Effect of pyrolysis temperature on physicochemical properties and hexavalent chromium adsorption of corncob biochars. *Biomass Conversion and Biorefinery, 13(3)*, 15197–15210. doi: https://doi.org/10.1007/s13399-023-05018-7

Shen, J. &. (2004). Effects of temperature and pH on adsorption isotherms for cupric and cadmium ions in single and binary solutions using corncob particles as adsorbent. *Separation Science and Technology, 39*, 3023–3041. doi: https://doi.org/10.1081/SS-200030335

Šimůnek, J. J. (2013). Numerical modeling of contaminant transport using HYDRUS and its specialized modules. *Journal of the Indian Institute of Science*, 265–284.

Spokas, K. A. (2012). Biochar's role as an alternative N-fertilizer: Ammonia capture. *Plant and Soil, 350(1–2)*, 35–42. doi:https://doi.org/10.1007/s11104-011-0930-8

Sud, D. M. (2008). Agricultural waste material as potential adsorbent for sequestering heavy metal ions from aqueous solutions: a review. *Bioresource Technology*, 6017–6027. doi: https://doi.org/10.1016/j.biortech.2007.11.064

Tong, Y. M. (2019). Adsorption of organic micropollutants onto biochar: A review of relevant kinetics, mechanisms and equilibrium. *Environmental Science: Water Research & Technology, 5*, 821–838. doi:https://doi.org/10.1039/C8EW00938D

Tudi, M. R. (2021). Agriculture Development, Pesticide Application and Its Impact on the Environment. *International Journal of Environmental Research and Public Health, 18(3)*, 1112. doi: https://doi.org/10.3390/ijerph18031112

Wu, F.-C. T.-L.-S. (2009). Characteristics of Elovich equation used for the analysis of adsorption kinetics in dye-chitosan systems. *Chemical Engineering Journal*, 366–373. doi: https://doi.org/10.1016/j.cej.2009.01.014

Ye, M. B. (2017). Pesticide exposures and respiratory health in general populations. *Journal of Environmental Sciences (China), 51*, 361–370. doi:https://doi.org/10.1016/j.jes.2016.11.012

Zendzian, R. (2003). Pesticide residue on/in the washed skin and its potential contribution to dermal toxicity. *Journal of Applied Toxicology, 23(2)*, 121–136. doi:https://doi.org/10.1002/jat.900

Zhang, . A. (2024). Food waste biochar: a sustainable solution for agriculture application and soil-water remediation. *Sustainable Agriculture Reviews (Springer)*. doi:https://doi.org/10.1007/s44246-024-00123-2

6 List of Figures

7 List of Tables